Inorg. Chem. **2004**, *43*, 6905–6921

X-ray Crystal Structures of $[XF_6][Sb_2F_{11}]$ (X = Cl, Br, I); ^{35,37}Cl, ^{79,81}Br, and ^{127}I NMR Studies and Electronic Structure Calculations of the XF_6^+ Cations

John F. Lehmann,[†] Gary J. Schrobilgen,*[,†] Karl O. Christe,[‡] Andreas Kornath,[‡] and Reijo J. Suontamo[§]

Department of Chemistry, McMaster University, Hamilton, Ontario, L8S 4M1, Canada, Loker Hydrocarbon Research Institute, University of Southern California, University Park, Los Angeles, California 93524, and University of Jyväskylä, P.O. Box 35, FIN-40351 Jyväskylä, Finland

Received February 2, 2004

The single-crystal X-ray structures of $[XF_6][Sb_2F_{11}]$ (X = Cl, Br, I) have been determined and represent the first detailed crystallographic study of salts containing the XF_6^+ cations. The three salts are isomorphous and crystallize in the monoclinic space group $P2_1/n$ with $Z = 4$: $[ClF_6][Sb_2F_{11}]$, $a = 11.824(2)$ Å, $b = 8.434(2)$ Å, $c = 12.088(2)$ Å, $\beta = 97.783(6)°$, $V = 1194.3(4)$ Å^3, $R_1 = 0.0488$ at –130 °C; $[BrF_6][Sb_2F_{11}]$, $a = 11.931(2)$ Å, $b = 8.492(2)$ Å, $c = 12.103(2)$ Å, $\beta = 97.558(4)°$, $V = 1215.5(4)$ Å^3, $R_1 = 0.0707$ at –130 °C; $[IF_6][Sb_2F_{11}]$, $a = 11.844(1)$ Å, $b = 8.617(1)$ Å, $c = 11.979(2)$ Å, $\beta = 98.915(2)°$, $V = 1207.8(3)$ Å^3, $R_1 = 0.0219$ at –173 °C. The crystal structure of $[IF_6][Sb_2F_{11}]$ was also determined at –100 °C and was found to crystallize in the monoclinic space group $P2_1/m$ with $Z = 4$, $a = 11.885(1)$ Å, $b = 8.626(1)$ Å, $c = 12.000(1)$ Å, $\beta = 98.44(1)$, $V = 1216.9(2)$ Å^3, $R_1 = 0.0635$. The XF_6^+ cations have octahedral geometries with average Cl–F, Br–F, and I–F bond lengths of 1.550(4), 1.666(11) and 1.779(6) [–173 °C]/1.774(8) [–100 °C] Å, respectively. The chemical shifts of the central quadrupolar nuclei, ^{35,37}Cl, ^{79,81}Br, and ^{127}I, were determined for $[ClF_6][AsF_6]$ (814 ppm), $[BrF_6][AsF_6]$ (2080 ppm), and $[IF_6][Sb_3F_{16}]$ (3381 ppm) in anhydrous HF solution at 27 °C, and spin-inversion-recovery experiments were used to determine the T_1-relaxation times of ^{35}Cl (1.32(3) s), ^{37}Cl (2.58(6) s), ^{79}Br (24.6(4) ms), ^{81}Br (35.4(5) ms), and ^{127}I (6.53(1) ms). Trends among the central halogen chemical shifts and T_1-relaxation times of XF_6^+, XO_4^-, and X^- are discussed. The isotropic ^1J-coupling constants and reduced coupling constants for the XF_6^+ cations and isoelectronic hexafluoro species of rows 3–6 are empirically assessed in terms of the relative contributions of the Fermi-contact, spin–dipolar, and spin–orbit mechanisms. Electronic structure calculations using Hartree–Fock, MP2, and local density functional methods were used to determine the energy-minimized gas-phase geometries, atomic charges, and Mayer bond orders of the XF_6^+ cations. The calculated vibrational frequencies are in accord with the previously published assignments and experimental vibrational frequencies of the XF_6^+ cations. Bonding trends within the XF_6^+ cation series have been discussed in terms of natural bond orbital (NBO) analyses, the ligand close-packed (LCP) model, and the electron localization function (ELF).

Introduction

Iodine heptafluoride, the only known halogen heptafluoride, exhibits amphoteric behavior, reacting with suitable fluoride ion donors and acceptors to form the IF_8^- and IF_6^+ ions, respectively. The IF_6^+ cation was first prepared as its AsF_6^- and $Sb_3F_{16}^-$ salts by the reaction of IF_7 with AsF_5[1,2] and SbF_5.[2] The coordinatively saturated natures of the ClF_6^+ and BrF_6^+ cations require that they be prepared by the oxidative fluorination of ClF_5 (or ClO_2F) and BrF_5. Although PtF_6 oxidizes ClF_5 [3–5] or ClO_2F[4,5] to $[ClF_6][PtF_6]$ in ap-

* Author to whom correspondence should be addressed. E-mail: schrobil@mcmaster.ca.
[†] McMaster University.
[‡] University of Southern California.
[§] University of Jyväskylä.

(1) Seel, F.; Detmer, O. *Angew. Chem.* **1958**, *70*, 163.
(2) Seel, F.; Detmer, O. *Z. Anorg. Allg. Chem.* **1959**, *301*, 113.
(3) Roberto, F. Q. *Inorg. Nucl. Chem. Lett.* **1972**, *8*, 737.

10.1021/ic040015o CCC: $27.50
Published on Web 07/01/2004

proximately 17% yield with respect to PtF_6 (eqs 1−3), no means of separating $[ClF_6][PtF_6]$ from the chlorine(III) and -(V) byproducts has been devised. In contrast, PtF_6 is

$$2ClF_5 + 2PtF_6 \xrightarrow{\text{unfiltered UV}} [ClF_6][PtF_6] + [ClF_2][PtF_6] + F_2 \quad (1)$$

$$2ClF_5 + 2PtF_6 \xrightarrow{\text{filtered UV}} [ClF_6][PtF_6] + [ClF_4][PtF_6] \quad (2)$$

$$6ClO_2F + 6PtF_6 \xrightarrow{-78\ ^\circ C} [ClF_6][PtF_6] + 5[ClO_2][PtF_6] + O_2 \quad (3)$$

incapable of oxidizing BrF_5 to BrF_6^+ under similar, or photolytic conditions,[6] which is consistent with the general reluctance of bromine and other late row 4 elements to achieve their highest oxidation states.[7] The salts, $[ClF_6][AsF_6]$[8] and $[BrF_6][AsF_6]$,[6] can be obtained in high purity, but in low yields (ca. 11 and <20%, respectively), by oxidative fluorination of ClF_5 and BrF_5 with $[KrF][AsF_6]$ or $[Kr_2F_3][AsF_6]$ (eqs 4, 5). The $[ClF_4][AsF_6]$ and $[BrF_4][AsF_6]$

$$XF_5 + [KrF][AsF_6] \rightarrow [XF_6][AsF_6] + Kr \quad (X = Cl, Br) \quad (4)$$

$$XF_5 + [Kr_2F_3][AsF_6] \rightarrow [XF_6][AsF_6] + KrF_2 + Kr \quad (X = Cl, Br) \quad (5)$$

salts are obtained as side products in these reactions as a consequence of the autodecomposition of $[KrF][AsF_6]$ and $[Kr_2F_3][AsF_6]$ to Kr, F_2, and AsF_5, and the subsequent reaction of AsF_5 with the halogen pentafluoride; however, both salts have significant dissociation vapor pressures at ambient temperature and can be removed from the nonvolatile $[XF_6][AsF_6]$ (X = Cl, Br) salts under dynamic vacuum.[6,8] The $[XF_6][AsF_6]$ (X = Cl, Br) salts can be prepared in higher yields (ca. 42% and 32%, respectively) using the thermodynamically unstable oxidant, NiF_3^+, prepared in situ by reaction of NiF_6^{2-} with AsF_5 in anhydrous HF (eq 6).[9]

$$[Cs]_2[NiF_6] + 5AsF_5 + XF_5 \rightarrow [XF_6][AsF_6] + [Ni][AsF_6]_2 + 2[Cs][AsF_6] \quad (X = Cl, Br) \quad (6)$$

Although $[ClF_6][AsF_6]$ and $[BrF_6][AsF_6]$ can be separated from $[Ni][NiF_6]$ and $[Cs][AsF_6]$ on the basis of the solubilities of the products in HF, the $[XF_6][AsF_6]$ salts prepared by this method are generally of lower purity than when prepared using $[KrF][AsF_6]$ or $[Kr_2F_3][AsF_6]$.[9]

The vibrational spectra of salts containing the ClF_6^+,[3−5,8−10] BrF_6^+,[6,9,11] and IF_6^+ [12−15] cations have been reported and are consistent with octahedral symmetries for each member of the series. The ^{19}F NMR spectra of ClF_6^+,[4,5,8,9] BrF_6^+,[6,9] and IF_6^+ [15,16] and the ^{127}I NMR spectrum of IF_6^+ [16] in anhydrous HF solution exhibit well-resolved halogen−fluorine spin−spin couplings, which are indicative of near-zero electric field gradients at the quadrupolar $^{35,37}Cl$ ($I = {}^3/_2$), $^{79,81}Br$ ($I = {}^3/_2$), and ^{127}I ($I = {}^5/_2$) nuclei that arise as a consequence of their octahedral coordination. Spin−spin couplings have also been observed in the ^{19}F and ^{127}I NMR spectra of powdered $[IF_6][AsF_6]$;[17] however, minor distortions of the cation in the solid state result in partial quadrupolar collapse of the signals and much broader line widths. Powder X-ray diffraction studies of $[ClF_6][AsF_6]$,[8] $[BrF_6][AsF_6]$,[11] and $[IF_6][AsF_6]$[12,18] have not afforded detailed structural information about the XF_6^+ cations; however, the cubic morphologies of these salts (space group, *Pa*3) are consistent with the octahedral geometries of the XF_6^+ and AsF_6^- ions.

The present study provides the first detailed structural characterization of the XF_6^+ cations by single-crystal X-ray diffraction. The solid-state structures of the XF_6^+ cations and their previously reported vibrational frequencies are compared with those calculated using the Hartree−Fock (HF), MP2, and LDF methods. These calculations have been used, in conjunction with electron localization functions, to assess the electronic structures and bonding of the XF_6^+ (X = Cl, Br, I) cation series. The spectroscopic characterizations of the XF_6^+ cations have been extended to include the ^{35}Cl, ^{37}Cl, ^{79}Br, ^{81}Br, and ^{127}I solution NMR spectra of $[ClF_6][AsF_6]$, $[BrF_6][AsF_6]$, and $[IF_6][Sb_3F_{16}]$, and the determination of the spin−lattice relaxation times (T_1) of these central nuclei for the XF_6^+ cations.

Results and Discussion

The $Sb_2F_{11}^-$ salts of ClF_6^+, BrF_6^+, and IF_6^+ were chosen for investigation by X-ray diffraction over the more easily prepared AsF_6^- salts for two reasons: (1) the electron density of arsenic is very similar to that of bromine and would not allow for easy differentiation between the octahedral BrF_6^+ and AsF_6^- ions in the Fourier difference maps during the refinement of the crystal structure of $[BrF_6][AsF_6]$ (a similar problem would be encountered for $[IF_6][SbF_6]$), and (2) the AsF_6^- salts have been shown by powder diffraction to crystallize in the cubic space group, *Pa*3,[8,11,12] and may be prone to disorder as a result of the high unit cell symmetry. Salts of other octahedral anions, such as SbF_6^-, and PtF_6^-, were avoided for similar reasons. The use of the $Sb_2F_{11}^-$ anion avoids both of the aforementioned problems because of its nonoctahedral geometry and the reduced unit cell symmetry of the $[XF_6][Sb_2F_{11}]$ salts (space group, $P2_1/n$). Furthermore, the $Sb_2F_{11}^-$ salts crystallize selectively from anhydrous HF when the mole ratio SbF_5:$[XF_6][SbF_6] \geq 1$.

(4) Christe, K. O. *Inorg. Nucl. Chem. Lett.* **1972**, *8*, 741.
(5) Christe, K. O. *Inorg. Chem.* **1973**, *12*, 1580.
(6) Gillespie, R. J.; Schrobilgen, G. J. *Inorg. Chem.* **1974**, *13*, 1230.
(7) Huheey, J. E. *Inorganic Chemistry*, 4th ed.; HarperCollins College Publishers: New York, 1993; pp 876−877.
(8) Christe, K. O.; Wilson, W. W.; Curtis, E. C. *Inorg. Chem.* **1983**, *22*, 3056.
(9) Schroer, T.; Christe, K. O. *Inorg. Chem.* **2001**, *40*, 2415.
(10) Christe, K. O.; Wilson, W. W. *Inorg. Chem.* **1983**, *22*, 1950.
(11) Christe, K. O.; Wilson, R. D. *Inorg. Chem.* **1975**, *14*, 694.
(12) Christe, K. O.; Sawodny, W. *Inorg. Chem.* **1967**, *6*, 1783.
(13) Christe, K. O. *Inorg. Chem.* **1970**, *9*, 2801.
(14) Christe, K. O.; Sawodny, W. *Inorg. Chem.* **1968**, *7*, 1685.
(15) Brownstein, M.; Selig, H. *Inorg. Chem.* **1972**, *11*, 656.
(16) Dove, M. F. A.; Sanders, J. C. P.; Appelman, E. H. *Magn. Reson. Chem.* **1995**, *33*, 44.
(17) Hon, J. F.; Christe, K. O. *J. Chem. Phys.* **1970**, *52*, 1960.
(18) Beaton, S. Ph.D. Thesis, University of British Columbia, 1966. The I−F bond length was estimated to be 1.75 Å from powder diffraction data.

Table 1. Summary of Crystal Data and Refinement Results for $[ClF_6][Sb_2F_{11}]$, $[BrF_6][Sb_2F_{11}]$, and $[IF_6][Sb_2F_{11}]$

	$[ClF_6]$-$[Sb_2F_{11}]$	$[BrF_6]$-$[Sb_2F_{11}]$	$[IF_6]$-$[Sb_2F_{11}]$	$[IF_6]$-$[Sb_2F_{11}]$
space group	$P2_1/n$	$P2_1/n$	$P2_1/n$	$P2_1/m$
a (Å)	11.824(2)	11.931(2)	11.844(1)	11.885(1)
b (Å)	8.434(2)	8.492(2)	8.617(1)	8.626(1)
c (Å)	12.088(2)	12.103(2)	11.979(2)	12.000(1)
β (deg)	97.783(6)	97.558(6)	98.915(2)	98.44(1)
V (Å^3)	1194.3(4)	1215.5(4)	1207.8(3)	1216.9(2)
Z	4	4	4	4
mol wt (g mol^{-1})	601.93	646.38	693.40	693.40
ρ_{calcd} (g cm^{-3})	3.348	3.969	3.813	3.785
T (°C)	−130	−130	−173	−100
μ (mm^{-1})	4.95	11.23	7.23	7.181
R_1[a]	0.0488	0.0707	0.0217	0.0635
wR_2[b]	0.1070	0.1577	0.0601	0.1689

[a] $R_1 = \sum||F_o| - |F_c||/\sum|F_o|$ for $I > 2\sigma(I)$. [b] $wR_2 = \sum|(|F_o| - |F_c|)w^{1/2}|/\sum(|F_o|w)$ for $I > 2\sigma(I)$.

Syntheses of $[ClF_6][AsF_6]$, $[ClF_6][Sb_2F_{11}]$, $[BrF_6][AsF_6]$, $[BrF_6][Sb_2F_{11}]$, and $[IF_6][Sb_3F_{16}]$. The salts $[ClF_6][AsF_6]$[8] and $[BrF_6][AsF_6]$[6] were prepared by oxidation of ClF_5 and BrF_5 with $[KrF][AsF_6]$ at ambient temperature as previously described. The salt $[IF_6][Sb_3F_{16}]$ was prepared by the reaction of IF_7 with excess SbF_5 (eq 7), and $[IF_6][Sb_2F_{11}]$, used for

$$IF_7 + 3SbF_5 \rightarrow [IF_6][Sb_3F_{16}] \quad (7)$$

its crystal structure determination at −100 °C (vide infra), was similarly prepared by the reaction of IF_7 with 2 molar equiv of SbF_5 in anhydrous HF. These salts were dissolved in anhydrous HF for the NMR studies. The $[XF_6][Sb_2F_{11}]$ (X = Cl, Br) salts, used for the crystallographic studies, were prepared from $[XF_6][AsF_6]$ by the displacement of AsF_5 with SbF_5 in anhydrous HF (eq 8). Crystals of $[XF_6][Sb_2F_{11}]$

$$[XF_6][AsF_6] + 2SbF_5 \rightarrow [XF_6][Sb_2F_{11}] + AsF_5 \quad (X = Cl, Br) \quad (8)$$

(X = Cl, Br, I) suitable for X-ray crystallography were grown by slowly cooling HF solutions of $[XF_6][Sb_2F_{11}]$ (X = Cl, Br) and $[IF_6][Sb_3F_{16}]$.

X-ray Crystal Structures of $[XF_6][Sb_2F_{11}]$ (X = Cl, Br, I). The unit cell parameters and refinement statistics for $[ClF_6][Sb_2F_{11}]$, $[BrF_6][Sb_2F_{11}]$, and $[IF_6][Sb_2F_{11}]$ are given in Table 1. The bond lengths, contact distances, and bond angles determined for $[ClF_6][Sb_2F_{11}]$, $[BrF_6][Sb_2F_{11}]$, and $[IF_6][Sb_2F_{11}]$[19] are summarized in Table 2.

The crystal structures of $[ClF_6][Sb_2F_{11}]$ (−130 °C), $[BrF_6]$-$[Sb_2F_{11}]$ (−130 °C), and $[IF_6][Sb_2F_{11}]$ (−173 °C) (Figure 1) are isomorphous, and were solved in the monoclinic space group $P2_1/n$ ($Z = 4$), whereas the crystal structure of $[IF_6]$-$[Sb_2F_{11}]$ at −100 °C was solved in the monoclinic space group $P2_1/m$ ($Z = 4$). The structures consist of $Sb_2F_{11}^-$ anions, which lie on general positions, and two XF_6^+ cations, one of which lies on the origin, and the second lies in the center of the $b-c$ face of the unit cell. The packing of the

(19) The structure of $[IF_6][Sb_2F_{11}]$ at −100 °C was solved in the space group $P2_1/m$, but exhibited higher thermal parameters for the equatorial fluorine positions of the anion and significantly higher values of R_1 and wR_2. For these reasons, the discussion of the metric parameters of $[IF_6][Sb_2F_{11}]$ is limited to those determined at −173 °C.

Table 2. Summary of Bond Lengths, Contact Distances and Bond Angles for $[ClF_6][Sb_2F_{11}]$, $[BrF_6][Sb_2F_{11}]$, and $[IF_6][Sb_2F_{11}]$

	$[ClF_6]$-$[Sb_2F_{11}]$	$[BrF_6]$-$[Sb_2F_{11}]$	$[IF_6]$-$[Sb_2F_{11}]$	$[IF_6]$-$[Sb_2F_{11}]$[a]
Bond Lengths (Å)				
X(1)−F(1)	1.558(4)	1.684(9)	1.778(8)	1.767(7)
X(1)−F(2)	1.548(4)	1.657(9)	1.779(8)	1.780(10)
X(1)−F(3)	1.548(5)	1.659(8)	1.774(3)	1.771(7)
X(2)−F(4)	1.551(5)	1.664(10)	1.789(7)	1.782(6)
X(2)−F(5)	1.547(4)	1.657(8)	1.773(2)	1.775(9)
X(2)−F(6)	1.550(4)	1.674(9)	1.779(8)	1.769(6)
Sb(1)−F(7)	1.852(4)	1.847(9)	1.865(2)	
Sb(1)−F(8)	1.850(5)	1.838(10)	*b*	
Sb(1)−F(9)	1.841(5)	1.873(10)	*b*	
Sb(1)−F(10)	1.846(5)	1.855(11)	*b*	
Sb(1)−F(11)	1.857(6)	1.844(11)	*b*	
Sb(1)−F(12)	2.045(4)	2.046(9)	2.057(2)	
Sb(2)−F(12)	2.019(4)	2.028(8)	2.033(2)	
Sb(2)−F(13)	1.864(4)	1.858(9)	1.866(2)	
Sb(2)−F(14)	1.852(5)	1.850(9)	1.841(8)	
Sb(2)−F(15)	1.855(5)	1.854(10)	1.854(7)	
Sb(2)−F(16)	1.862(4)	1.864(9)	1.870(8)	
Sb(2)−F(17)	1.843(5)	1.838(9)	1.869(8)	
Intracation Contact Distances (Å)[c]				
F(1)···F(2)	2.194	2.362	2.522	
F(1)···F(3)	2.193	2.348	2.503	
F(1)···F(2A)	2.198	2.363	2.510	
F(1)···F(3A)	2.200	2.379	2.521	
F(2)···F(3)	2.199	2.351	2.527	
F(2)···F(3A)	2.180	2.338	2.497	
F(4)···F(5)	2.190	2.352	2.517	
F(4)···F(6)	2.192	2.367	2.554	
F(4)···F(5A)	2.190	2.344	2.520	
F(4)···F(6A)	2.193	2.353	2.492	
F(5)···F(6)	2.192	2.356	2.526	
F(5)···F(6A)	2.187	2.355	2.497	
Interionic Contact Distances (Å)[b]				
F(1)···F(8)	2.746	2.777	2.551[d]	
F(1) ···F(13)	2.914	2.911	2.802	
F(2)···F(8)	2.934	[2.959]	2.893[d]	
F(2)···F(13)	2.771	2.801	2.784	
F(2)···F(11)	2.743	2.789	2.704[d]	
F(3)···F(8)	2.877	2.872	2.654[d]	
F(3)···F(9)	2.846	2.871	2.769[d]	
F(4)···F(7)	2.831	2.878	[2.984]	
F(4)···F(16)	2.766	2.757	2.781	
F(4)···F(15)	2.870	2.911	2.882	
F(5)···F(17)	2.688	2.679	[2.974]	
F(5)···F(15)	2.905	2.913	[3.046]	
F(5)···F(13)	[2.998]	[2.946]	2.836	
F(6)···F(7)	2.920	2.901	[2.962]	
F(6)···F(10)	2.599	2.567	2.722[d]	
F(6)···F(16)	2.916	2.914	2.904	
F(6)···F(15)	2.809	2.810	2.732	
X(1)···F(8)	[3.451]	[3.483]	3.401[d]	
X(1)···F(9)	[3.541]	[3.560]	3.412[d]	
X(1)···F(13)	[3.515]	[3.527]	3.435	
X(1)···F(11)	[3.715]	[3.812]	[3.923]	
X(2)···F(7)	[3.522]	[3.547]	[3.579]	
X(2)···F(16)	[3.540]	[3.554]	[3.491]	
X(2)···F(15)	[3.460]	[3.493]	[3.870]	
X(2)···F(13)	[4.061]	[4.059]	[3.499]	
Bond Angles (deg)				
F(1)−X(1)−F(2)	89.9(3)	90.0(5)	90.3(1)	
F(1)−X(1)−F(3)	90.2(3)	89.3(5)	89.6(4)	
F(2)−X(1)−F(3)	90.5(3)	90.3(5)	90.7(4)	
F(4)−X(2)−F(5)	90.0(3)	90.2(5)	89.9(4)	
F(4)−X(2)−F(6)	90.0(3)	90.4(5)	91.4(1)	
F(5)−X(2)−F(6)	90.1(2)	90.0(5)	90.7(4)	
Sb(1)−F(12)−Sb(2)	145.2(3)	144.7(4)	144.1(1)	

[a] Metric parameters for the two crystallographically nonequivalent $Sb_2F_{11}^-$ anions may be found in the Supporting Information (CIF). [b] The equatorial Sb(1)−F(8−11) bonds of the 4-fold disordered $-SbF_5$ group have bond lengths ranging from 1.72(2) to 1.92(2) Å. [c] Contact distances given in square brackets exceed the sum of the van der Waals radii, but are provided for comparison. [d] The F···F and I···F contact distances to F(8−11) correspond to the shortest distances of the modeled 4-fold disorder.

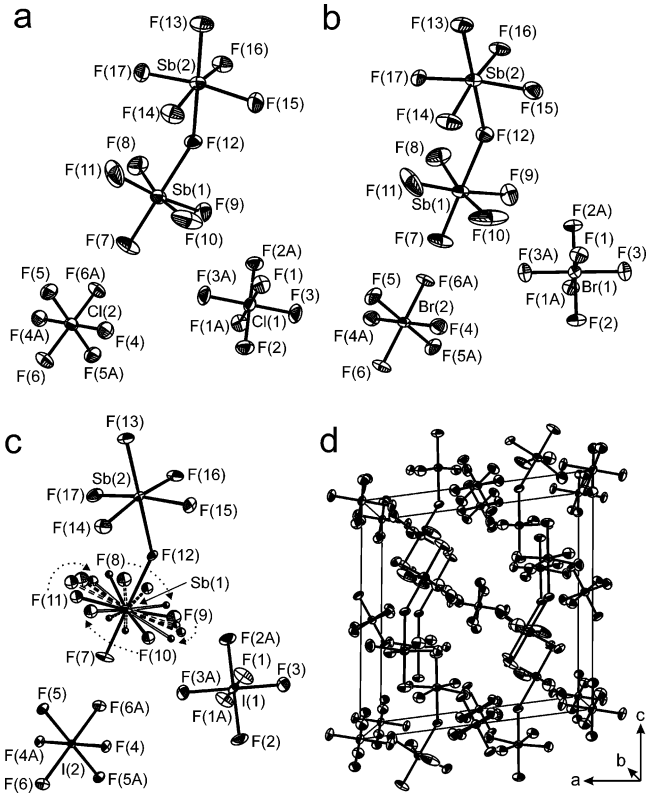

Figure 1. The crystal structures of (a) $[ClF_6][Sb_2F_{11}]$ (−130 °C), (b) $[BrF_6][Sb_2F_{11}]$ (−130 °C), and (c) $[IF_6][Sb_2F_{11}]$ (−173 °C). The packing diagram of (d) $[ClF_6][Sb_2F_{11}]$ is representative of the three $[XF_6][Sb_2F_{11}]$ (X = Cl, Br, I) salts. The thermal ellipsoids are shown at the 50% probability level.

$[XF_6][Sb_2F_{11}]$ salts is best described in terms of layers of XF_6^+ cations and $Sb_2F_{11}^-$ anions lying parallel to the $b-c$ face of the unit cell (Figure 1d). It is noteworthy that the unit cell volume increases on going from $[ClF_6][Sb_2F_{11}]$ (1194.3(4) Å^3) to $[BrF_6][Sb_2F_{11}]$ (1215.5(4) Å^3), but decreases slightly from $[BrF_6][Sb_2F_{11}]$ to $[IF_6][Sb_2F_{11}]$ (1207.8(3) Å^3). The contraction of the $[IF_6][Sb_2F_{11}]$ unit cell may be attributed, in part, to the lower data acquisition temperature (−173 °C) used for this salt when compared with that used for the lighter halogen analogues (−130 °C); however, at −100 °C, the unit cell volume of $[IF_6][Sb_2F_{11}]$ (1216.9(2) Å^3) is comparable to that of $[BrF_6][Sb_2F_{11}]$ at −130 °C. For comparison, the unit cell volumes of $[XF_6][AsF_6]$ obtained at 22 °C increase in the order $[BrF_6][AsF_6]$ (829.0 Å^3)[8] < $[ClF_6][AsF_6]$ (849.3 Å^3)[11] < $[IF_6][AsF_6]$ (854.7 Å^3).[12] Thus, the unit cell volume is not rigorously dependent upon the cation size, but is also influenced by the packing efficiency of the ions in the solid state (vide infra).

Although the XF_6^+ cations are constrained to local C_i site symmetries by the $P2_1/n$ space group, the *cis*-F−X−F bond angles were not differentiable from 90° at the $\pm 3\sigma$ (99.7%) confidence limit (Table 2). The average X−F bond lengths (Cl−F, 1.550(4) Å; Br−F, 1.666(11) Å; I−F, 1.779(6) Å) increase in a near-linear manner with increasing atomic number, Z_X, of the central halogen atom. The ranges of the intra-ionic F···F distances in ClF_6^+ (2.180−2.200 Å), BrF_6^+ (2.338−2.379 Å), and IF_6^+ (2.492−2.554 Å) are small, with the average F···F distance increasing down the group, reflecting the increasing size and ability of the central halogen valence shell to accommodate higher coordination numbers (see Assessment of Ligand Close Packing Among the Hexafluoro-Species of Groups 14−17).

The XF_6^+ cations have 13−16 interionic F···F contacts to neighboring anions that lie within twice the van der Waals radius of fluorine (2.70,[20] 2.94 Å[21]) (Table 2). The interionic F···F contact distances are comparable in the three XF_6^+ salts investigated, ranging from 2.60, 2.57, and 2.55 to 2.93, 2.91, and 2.90 Å for $[ClF_6][Sb_2F_{11}]$, $[BrF_6][Sb_2F_{11}]$, and $[IF_6][Sb_2F_{11}]$, respectively. The large number of long contacts and the formal negative charges on the interacting fluorine atoms suggest that these cation−anion interactions are diffuse and nondirectional; consequently, significant distortions of the octahedral XF_6^+ cations are not observed. Although all three XF_6^+ cations have six F···X contacts between the fluorine atoms of the anions and the central halogen atoms that are close to the sum of the fluorine (1.35,[20] 1.47 Å[21]) and central halogen (Cl, 1.80,[20] 1.75;[21] Br, 1.95,[20] 1.85;[21] I, 2.15,[20] 1.98 Å[21]) van der Waals radii, the shortest are observed for $[IF_6][Sb_2F_{11}]$ (Table 2). In addition, there are two longer F···X contacts that approach the centers of two triangular faces of each cation octahedron that are trans to each other (Table 2). The shorter I···F contacts to the $Sb_2F_{11}^-$ anions may contribute to the contraction of the $[IF_6][Sb_2F_{11}]$ unit cell volume relative to that of $[BrF_6][Sb_2F_{11}]$ (Table 1).

The equatorial fluorine atoms of the $Sb_2F_{11}^-$ anions of the ClF_6^+ and BrF_6^+ salts have staggered conformations with respect to each other. In contrast, the $Sb_2F_{11}^-$ anion of the IF_6^+ salt exhibits a 4-fold rotational disorder of the equatorial fluorine positions of Sb(1) about the F(7)−Sb(1)−F(12) axis (Figure 1c). This axis is nearly collinear with the 3-fold axis passing through the F(4), F(5), F(6) face of the cation. The superposition of the 3-fold symmetry of a cation face with the 4-fold symmetry of the Sb(1)−F(8−11) group does not afford an energetically favorable conformation for the fluorine atoms on the anion, and likely accounts for the observed disorder. In contrast the ordered equatorial Sb(2)−F(14−17) group of this salt is likely a consequence of the F(12)−Sb(2)−F(13) axis not being aligned with a 3-fold axis of the cation.

The Sb(1)−F(12)−Sb(2) bond angles lie within a narrow range for the $[XF_6][Sb_2F_{11}]$ salts (Cl, 145.2(3)°; Br, 144.7(4)°; I, 144.1(1)°). A recent computational study of the gas-phase geometry of the $Sb_2F_{11}^-$ anion has shown that the energy-minimized structure of the $Sb_2F_{11}^-$ anion has D_{4h} point symmetry, with a fluorine bridge angle of 180° and an eclipsed equatorial fluorine conformation.[22] The fluorine bridge angle was shown to be highly deformable, and the potential energy surface of the anion was shown to be insensitive to the relative conformations of equatorial fluorine atoms. Thus, the conformational geometry and fluorine bridge angle of the $Sb_2F_{11}^-$ anion are expected to be dependent on crystal packing. Edwards and co-workers[23−26]

(20) Pauling, L. *The Nature of the Chemical Bond*, 3rd ed.; Cornell University Press: Ithica, NY, 1960; p 260.
(21) Bondi, A. *J. Phys. Chem.* **1964**, *68*, 441.
(22) Sham, I. H. T.; Patrick, B. O.; von Ahsen, B.; von Ahsen, S.; Willner, H.; Thompson, R. C.; Aubke, F. *Solid State Sci.* **2002**, *4*, 1457.

have investigated the effects of the close packing arrangements of the light atoms in fluorine-bridged species. These studies showed that when the metal atoms lie within the octahedral interstitial sites of hexagonal close-packed oxygen and fluorine atoms, the ideal bridge bond angle is 132°. When the metal atom lies within the octahedral interstitial sites of a cubic close-packed lattice of oxygen and fluorine atoms, the ideal bridge bond angle is 180°. The fluorine atom packings and fluorine bridge angles in the $[XF_6][Sb_2F_{11}]$ salts most closely resemble hexagonal close packed-arrangements. Thus, the staggered and bent geometries of the anions in these salts may be attributed to solid-state packing effects.[27−29]

^{35,37}Cl, ^{79,81}Br, and ^{127}I NMR Parameters of XF_6^+ (X = Cl, Br, I). The quadrupolar natures of the ^{35,37}Cl ($I = {}^3/_2$), ^{79,81}Br ($I = {}^3/_2$), and ^{127}I ($I = {}^5/_2$) nuclides tend to produce extremely broad resonances as a consequence of the highly efficient quadrupolar relaxation mechanism, and generally do not allow the spectra of these nuclei to be exploited for chemical studies. Nevertheless, the few NMR studies in which the ^{35,37}Cl,[16,30−33] ^{79,81}Br,[16,34,35] and ^{127}I[16,17,31,34,36,37] nuclides have been employed have clearly demonstrated the usefulness of these nuclides, under certain conditions, for chemical characterization in solution. The relaxation of a quadrupolar nucleus, under the conditions of extreme narrowing, is described by eq 9, where $\Delta\nu_{1/2}$ is the line width at half-height; T_2 is the spin−spin relaxation time; T_1 is the spin−lattice relaxation time; I is the nuclear spin quantum number; Q is the nuclear quadrupole moment; eq is the electric field gradient (EFG); η is the asymmetry parameter for the EFG; and τ_c is the isotropic rotational correlation time.[38] Equation 9 reveals that line widths are dramatically

$$\Delta\nu_{1/2} = \frac{1}{\pi T_1} = \frac{1}{\pi T_2} = \left(\frac{3\pi}{10}\right)\left(\frac{2I+3}{I^2(2I-1)}\right)\left(\frac{eqQ}{h}\right)^2\left(1+\frac{\eta^2}{3}\right)\tau_c \quad (9)$$

reduced for nuclides having a high value of I, a small value of Q, or a combination of the two in accord with the line width factor, $(2I + 3)/[I^2(2I - 1)]Q^2$. The merits of the ^{35,37}Cl, ^{79,81}Br, and ^{127}I nuclides with regard to these requirements have been discussed previously.[16] Moreover, narrow line widths are known to arise from quadrupolar nuclei residing at the center of a highly symmetric ligand environment (e.g., O_h or T_d) for which the values of eq and η are low.[39] The local octahedral environments of the central halogen nuclides in the XF_6^+ (X = Cl, Br, I) cations have consequently allowed the characterization of all three hexafluoro cations in anhydrous HF solution by ^{35,37}Cl, ^{79,81}Br, and ^{127}I NMR spectroscopy in the present study.

The NMR spectra of the central halogen nuclei of $[^{35,37}ClF_6][AsF_6]$, $[^{79,81}BrF_6][AsF_6]$, and $[^{127}IF_6][Sb_3F_{16}]$ dissolved in anhydrous HF at 27 °C are shown in Figure 2. The ^{127}I NMR spectrum of the IF_6^+ cation has previously been reported for $[IF_6][AsF_6]$,[16] but has been obtained for $[IF_6][Sb_3F_{16}]$ in HF solvent in the present study, demonstrating that the anion has little effect on the chemical shift or $^1J(^{127}I-^{19}F)$. The ^{35}Cl, ^{37}Cl, ^{79}Br, ^{81}Br, and ^{127}I spectra of the XF_6^+ cations are binomial septets having intensity ratios of 1:6:15:20:15:6:1 as a consequence of coupling to the six chemically equivalent ^{19}F nuclei. The well-resolved $^1J(^{19}F-^mX)$ couplings are consistent with near-zero electric field gradients at the quadrupolar ^{35,37}Cl, ^{79,81}Br, and ^{127}I nuclei, and octahedral cation geometries.

(a) $^{35,37}ClF_6^+$, $^{79,81}BrF_6^+$, and $^{127}IF_6^+$ Spin−Lattice Relaxation Times. The ^{35,37}Cl, ^{79,81}Br, and ^{127}I spin−lattice relaxation times, T_1, for $[ClF_6][AsF_6]$, $[BrF_6][AsF_6]$, and $[IF_6][Sb_3F_{16}]$ in anhydrous HF solutions obtained by the spin-inversion-recovery technique for the ^{19}F-coupled cations are summarized in Table 3. The T_1-relaxation times for the ^{35}Cl (1.32(3) s), ^{37}Cl (2.58(6) s), ^{79}Br (24.6(4) ms), ^{81}Br (35.4(5) ms), and ^{127}I (6.53(1) ms) nuclei of the XF_6^+ cations were found to be somewhat longer than those reported for 0.1 to 1.4 M solutions of $[N(C_2H_5)_4][^{35}ClO_4]$ (0.810−1.150 s), $[N(C_2H_5)_4][^{79}BrO_4]$ (13.3−22.8 ms), and $[N(C_2H_5)_4][^{81}BrO_4]$ (18.7−31.9 ms) and 1.0 to 0.05 M solutions of $[N(C_2H_5)_4][^{127}IO_4]$ (3.9−6.1 ms) in CH_3CN.[16] The T_1-relaxation time obtained for $[IF_6][Sb_3F_{16}]$ is comparable to, but slightly smaller than, that previously obtained for $[IF_6][AsF_6]$ (9.7 ms) by use of line fitting techniques.[15,43] The T_1-relaxation times of the central quadrupolar halogen nuclei decrease with increasing width factor of the nuclide, with the values obtained in this study being similar to those obtained for the XO_4^- (X = Cl, Br, I) anions. The similar T_1-relaxation times determined for the central halogen nuclei of the XF_6^+ and XO_4^- ions are not surprising considering that both ions have cubic point symmetries, resulting in near-zero electric field gradients at the central nuclei. In addition to the highly symmetric environment around the central halogen atom, the

(23) Edwards, A. J.; Jones, G. R.; Sills, R. J. C. *J. Chem. Soc. A* **1970**, 2521.
(24) Edwards, A. J.; Steventon, B. R. *J. Chem. Soc. A* **1968**, 2503.
(25) Edwards, A. J.; Jones, G. R. *J. Chem. Soc. A* **1968**, 2511.
(26) Edwards, A. J.; Jones, G. R. *J. Chem. Soc. A* **1968**, 2074.
(27) Vij, A.; Tham, F. S.; Vij, V.; Wilson, W. W.; Christe, K. O. *Inorg. Chem.* **2002**, *41*, 6397.
(28) Minkwitz. R.; Reinemann, S.; Seelbinder, R.; Konikowski, D.; Hartl, H.; Brüdgam, I.; Hegge, J.; Hoge, B.; Sheehy, J. A.; Christe, K. O. *Inorg. Chem.* **2001**, *40*, 4404.
(29) Vij, A.; Wilson, W. W.; Vij, V.; Tham, F. S.; Sheehy, J. A.; Christe, K. O. *J. Am. Chem. Soc.* **2001**, *123*, 6308.
(30) Saito, Y. *Can. J. Chem.* **1965**, *43*, 2530.
(31) Lindman, B.; Forsén, S. In *NMR, Basic Principles and Progress*; Diehl, P., Fluck, E., Kosfeld, R., Eds.; Springer-Verlag: New York, 1976; Vol. 12, p 326.
(32) Drakenberg, T.; Forsén, S. In *The Multinuclear Approach to NMR Spectroscopy*; Lambert, J. B., Riddell, F. G., Eds.; NATO ASI Series C; Reidel: Boston, 1983; p 405.
(33) Lindman, B. In *NMR of Newly Accessible Nuclei*; Laszlo, P., Ed.; Academic Press: London, 1983; Vol. 1, p 233.
(34) Levason, W.; Ogden, J. S.; Spicer, M. D.; Young, N. A. *J. Chem. Soc., Dalton Trans.* **1990**, 349.
(35) Gillespie, R. J.; Spekkens, P. H. *Isr. J. Chem.* **1978**, *17*, 11.
(36) Kren, R. M.; Dodgen, H. W.; Nyman, C. J. *Inorg. Chem.* **1968**, *7*, 446.
(37) Evans, J.; Levason, W.; Spicer, M. D. *J. Chem. Soc., Dalton Trans.* **1990**, 2307.
(38) Abragam, A. *The Principles of Nuclear Magnetism*; Oxford University Press: London, 1978; Chapter 8.
(39) Sanders, J. C. P.; Schrobilgen, G. J. In *Multinuclear Magnetic Resonance in Liquids and Solids—Chemical Applications*; Granger, P., Harris, R. K., Eds.; Kluwer Academic Press: Netherlands, 1990; pp 157−186.
(40) Sundholm, D.; Olsen, J. *J. Chem. Phys.* **1993**, *98*, 7152.
(41) Legon, A. C.; Thorn, J. C. *Chem. Phys. Lett.* **1993**, *215*, 554.
(42) Bieroń, J.; Pyykoö, P.; Sundholm, D.; Kellö, V.; Sadlej, A. J. *Phys. Rev. A* **2001**, *64*, 1.
(43) Suzuki, M.; Kubo, R. *Mol. Phys.* **1963**, *7*, 201.

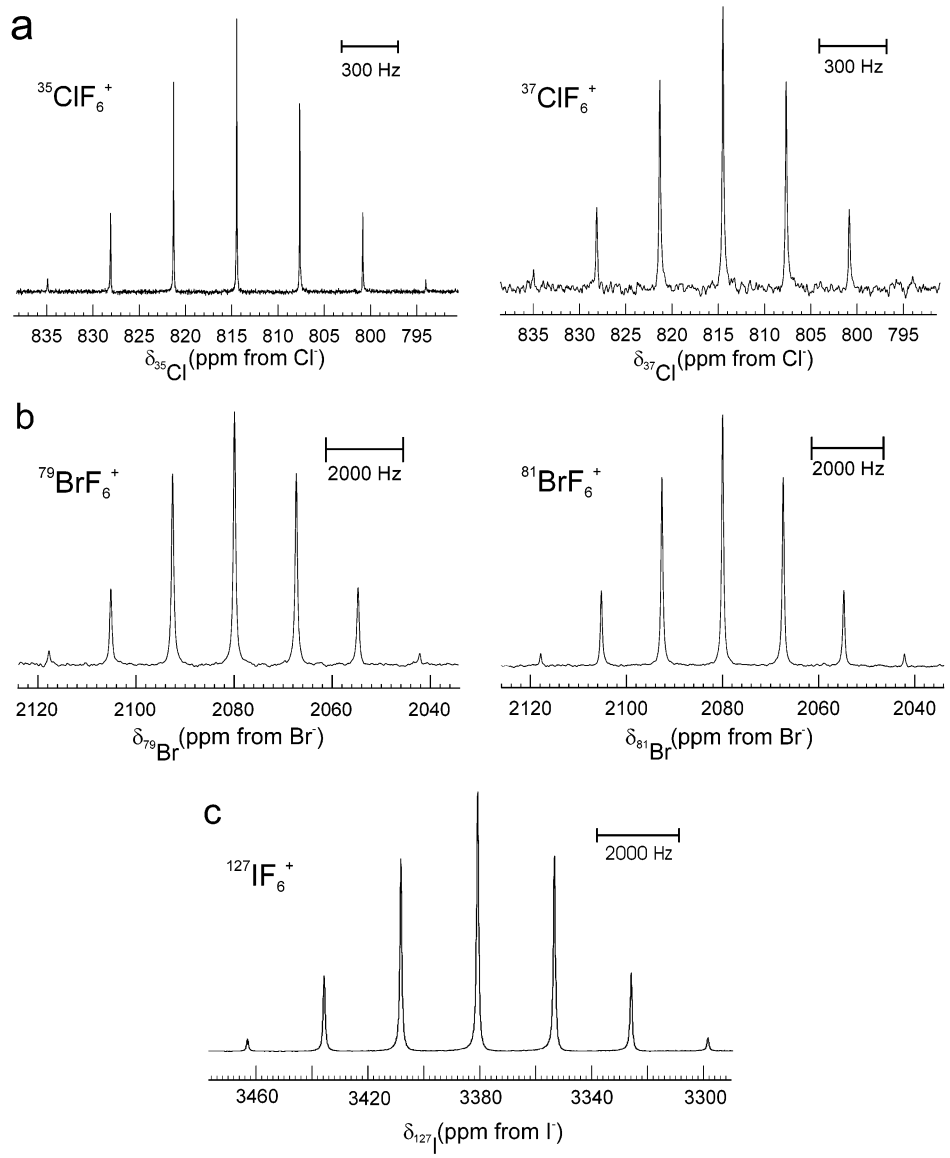

Figure 2. The (a) ^{35}Cl, ^{37}Cl, (b) ^{79}Br, ^{81}Br, and (c) ^{127}I NMR spectra of $[ClF_6][AsF_6]$, $[BrF_6][AsF_6]$, and $[IF_6][Sb_3F_{16}]$ in anhydrous HF at 27 °C.

Table 3. Spin−Lattice Relaxation Times (T_1) and Isotopic T_1 Ratios for $^{35,37}Cl$, $^{79,81}Br$, and ^{127}I of ClF_6^+, BrF_6^+, and IF_6^+ [a]

cation	T_1 (s)	Q (10^{-28} m^2)	T_1/T_1'	$(Q^2/Q'^2)^{-1}$	$\Delta\nu_{1/2}(X)_{obs}$ [b] (Hz)	$\Delta\nu_{1/2}(X)_{calcd}$ [c] (Hz)	$\Delta\nu_{1/2}(X)_{obs} - \Delta\nu_{1/2}(X)_{calcd}$ [c] (Hz)
$^{35}ClF_6^+$	1.32(3)	−0.08165(80)[d]	0.51(2)	0.621(9)	3.6	0.2	3.4
$^{37}ClF_6^+$	2.58(6)	−0.06435(64)[e]			3.2	0.1	3.1
$^{79}BrF_6^+$	0.0246(4)	0.313(3)[f]	0.69(2)	0.70(1)	25.0	12.9	12.1
$^{81}BrF_6^+$	0.0354(5)	0.262(3)[f]			16.8	9.0	7.8
$^{127}IF_6^+$	0.00653(1)	−0.710(10)[f]			55.5	48.8	6.7

[a] Data were obtained from the $^{35,37}Cl$, $^{79,81}Br$, and ^{127}I NMR spectra of $[ClF_6][AsF_6]$, $[BrF_6][AsF_6]$, and $[IF_6][Sb_3F_{16}]$ recorded in anhydrous HF solvent at 27 °C. [b] The line widths are given for the central line of each spectrum. [c] The line widths are calculated from $\Delta\nu_{1/2} = (\pi T_1)^{-1}$. [d] From ref 40. [e] From refs 40 and 41. [f] From ref 42.

comparatively large T_1 values of the XF_6^+ and XO_4^- ions are also attributed to the physical shielding of the central nuclei by their respective fluorine and oxygen ligands. Although this effect is not clearly evident when the T_1-relaxation times of XF_6^+ and XO_4^- are compared, the relaxation times of the spherically symmetric $^{35}Cl^-$ (23.8 ms), $^{81}Br^-$ (0.953 ms), and $^{127}I^-$ (0.190 ms) anions are significantly shorter[44] and may be attributed to electric field gradients induced by interactions with the aqueous solvent used in the latter studies and by larger rotational correlation times, τ_c, that result from solvation and ion-pair formation. The concentration dependence of T_1 was not investigated for the XF_6^+ cations; however, with the exception of $[ClF_6][AsF_6]$, the present solutions were more dilute than the most dilute solutions used for the T_1 investigations of the XO_4^- anions.[16] The use of dilute solutions minimizes ion-pairing effects, which, according to eq 9, should give rise to smaller τ_c values and longer T_1-relaxation times as noted in the T_1

(44) Hertz, H. G.; Holz, M.; Klute, R.; Stalidis, G.; Versmold, H. *Ber. Bunsen-Ges. Phys. Chem.* **1974**, *78*, 24.

determinations of XO_4^-. In addition to the concentration effect, a comparison of the XF_6^+ and XO_4^- T_1-relaxation times is complicated by the effect different solvent viscosities and dielectric constants have on τ_c and, hence, on T_1 in these studies.

If the T_1-relaxation time is dominated by the quadrupolar mechanism, then it follows from eq 9 that the line widths calculated from $\Delta\nu_{1/2} = (\pi T_1)^{-1}$ should equal those measured directly from the one-dimensional ^{35}Cl, ^{37}Cl, ^{79}Br, ^{81}Br, and ^{127}I NMR spectra. A comparison of the line widths obtained by the two methods (Table 3) reveals that the observed line widths are consistently greater than those derived from the T_1-relaxation times; however, the differences are small enough to support quadrupole relaxation as the dominant T_1-relaxation mechanism. The ^{127}I line width observed for [IF_6][Sb_3F_{16}] (55.5 Hz) is narrower than those reported for [IF_6][AsF_6] in HF solutions acidified with AsF_5 (170,[15] 70 Hz[16]). The $Sb_3F_{16}^-$ anion is expected to be extensively solvolyzed in HF, generating 2 molar equiv of SbF_5, which serves to acidify the solution. This trend is in agreement with the fluorine exchange mechanisms proposed by Brownstein and Selig[15] (eqs 10, 11), which are expected to be suppressed

$$IF_6^+ + HF_2^- \rightleftharpoons IF_7 + HF \qquad (10)$$

$$IF_6^+ + 2HF \rightleftharpoons IF_7 + H_2F^+ \qquad (11)$$

as the acidity of the HF solution increases. The minimal broadening of the central halogen line widths of [ClF_6][AsF_6] and [BrF_6][AsF_6] in HF solution in the absence of excess AsF_5 implies that ligand exchange routes analogous to those proposed in eqs 12 and 13 are unlikely for the ClF_6^+ and BrF_6^+ cations, and is consistent with the fact that ClF_7 and BrF_7 are unknown.

The dominance of the quadrupolar mechanism is further confirmed for the ^{35,37}Cl and ^{79,81}Br nuclei by considering the $T_1(^{35}\mathrm{Cl})/T_1(^{37}\mathrm{Cl})$ and $T_1(^{79}\mathrm{Br})/T_1(^{81}\mathrm{Br})$ ratios. These ratios should be inversely proportional to the Q^2 ratios of these nuclei multiplied by the spin factor ($f_I = (2I + 3)/(I^2(2I - 1))$) ratio as illustrated in eq 12. The nuclides ^{35}Cl, ^{37}Cl,

$$\frac{T_1(^{\mathrm{A}}\mathrm{X})}{T_1(^{\mathrm{B}}\mathrm{X})} = \left(\frac{f_I(^{\mathrm{B}}\mathrm{X})}{f_I(^{\mathrm{A}}\mathrm{X})}\right)\left(\frac{Q^2(^{\mathrm{B}}\mathrm{X})}{Q^2(^{\mathrm{A}}\mathrm{X})}\right) \qquad (12)$$

^{79}Br, and ^{81}Br each have a nuclear spin quantum number of $^3/_2$, which conveniently eliminates the spin-factor terms for these cations. For ClF_6^+, the ratio of the ^{35}Cl and ^{37}Cl T_1-relaxation times is 0.51(2) and is lower than the value of 0.621(9) estimated from the nuclear quadrupole moments of ^{35}Cl ($-0.08165(80) \times 10^{-28}$ m^2 A)[40] and ^{37}Cl ($-0.06435(64) \times 10^{-28}$ m^2 A).[40,41] The ratio of the ^{79}Br and ^{81}Br T_1-relaxation times is 0.69(2), and is in excellent agreement with the value of 0.70(1) calculated from the quadrupolar moments of ^{79}Br ($0.313(3) \times 10^{-28}$ m^2 A) and ^{81}Br ($0.262(3) \times 10^{-28}$ m^2 A).[42]

(b) ^{35,37}Cl, ^{79,81}Br, and ^{127}I Chemical Shifts. The ^{35,37}Cl, ^{79,81}Br, and ^{127}I chemical shifts obtained for the XF_6^+ cations are summarized in Table 4. The high-frequency chemical shifts of ^{35}Cl (814.3 ppm), ^{37}Cl (814.7 ppm), ^{79}Br (2079.9 ppm), ^{81}Br (2079.3 ppm), and ^{127}I (3380.6 ppm) are consistent with the high formal oxidation state of the central halogen and formal positive charge of the cation. The ^{127}I NMR chemical shift of [IF_6][Sb_2F_{11}] is slightly higher in frequency than that reported for [IF_6][AsF_6] (3361 ppm).[16] Despite the higher electronegativity of fluorine relative to that of oxygen, even higher frequency halogen chemical shifts are observed for $^{35}ClO_3^-$ (1050 ppm),[30] $^{35}ClO_4^-$ (1009 ppm),[16] $^{79,81}BrO_4^-$ (2489 ppm),[16] and $^{127}IO_4^-$ (4121 ppm),[16] and are presumably a consequence of the higher bond orders of the X−O bonds in the latter species.

Table 4. Chemical Shifts and Coupling Constants for XF_6^+ (X = Cl, Br, I)[a]

cation	$\delta(^{\mathrm{m}}\mathrm{X})$ (ppm)	$^1J(^{\mathrm{m}}\mathrm{X}-^{19}\mathrm{F})$ (Hz)	$^1K(\mathrm{X}-\mathrm{F})$ (10^{21} N A^{-2} m^{-3})
$^{35}ClF_6^+$	814.3	339	3.057
$^{37}ClF_6^+$	814.7	283	3.065
$^{79}BrF_6^+$	2079.9	1575	5.541
$^{81}BrF_6^+$	2079.3	1699	5.545
$^{127}IF_6^+$	3380.6	2744	12.046

[a] Parameters were obtained from the ^{35,37}Cl, ^{79,81}Br, and ^{127}I NMR spectra of [ClF_6][AsF_6], [BrF_6][AsF_6], and [IF_6][Sb_3F_{16}] recorded in anhydrous HF solvent at 27 °C.

The tendency for chemical shift ranges to increase with increasing atomic number within a group is well documented for the main-group and transition metal nuclides and has been correlated with the nonrelativistic and relativistic values of the radial terms, $\langle r^{-3}\rangle_{np}$ and $\langle r^{-3}\rangle_{nd}$, for the valence p and d electrons of the free atom.[45] The paramagnetic shielding term, which is proportional to $\langle r^{-3}\rangle_{np}$ and $\langle r^{-3}\rangle_{nd}$, dominates the chemical shifts of heavy nuclei as illustrated by the simple atom-in-a-molecule approach (eq 13),[45−47] where P_i and D_i represent the degrees of imbalance of valence electrons in the p and d orbitals, ΔE is the average excitation energy, μ_B is the Bohr magneton, and μ_o is the permeability of a vacuum.

$$\sigma^{\mathrm{p}} \approx -\left(\frac{\mu_o}{4\pi}\right)\left(\frac{4{\mu_B}^2}{\Delta E}\right)[\langle r^{-3}\rangle_{np} P_i + \langle r^{-3}\rangle_{nd} D_i] \qquad (13)$$

The relationships between the chemical shifts and the atomic numbers of the central halogen nuclei of X^-, XF_6^+, and XO_4^- illustrate that this trend holds for the halogens (Figure 3). Excluding the halide ions, X^-, which serve as chemical shift references for chlorine, bromine, and iodine, the relationships between chemical shift and Z_X are linear with positive slopes for both series. Both anion series also exhibit linear relationships between Z_X and $\langle {a_o}^3/r^3\rangle_{np}$, where values for $\langle {a_o}^3/r^3\rangle_{np}$ have been obtained from the atomic spectra of chlorine (7.16), bromine (13.55), and iodine (18.0).[48]

The dominance of the paramagnetic shielding terms in these species can also be assessed by comparing the ratios of the central halogen chemical shifts, referenced to the highly shielded X^- anions, where the paramagnetic shielding

(45) Jameson, C. J.; Gutowsky, H. S. *J. Chem. Phys.* **1964**, *40*, 1714.
(46) Griffith, J. S.; Orgel, L. E. *Trans. Faraday Soc.* **1957**, *53*, 601.
(47) Schneider, W. G.; Buckingham, A. D. *Discuss. Faraday Soc.* **1962**, *34*, 147.
(48) Barnes, R. G.; Smith, W. V. *Phys. Rev.* **1954**, *93*, 95.

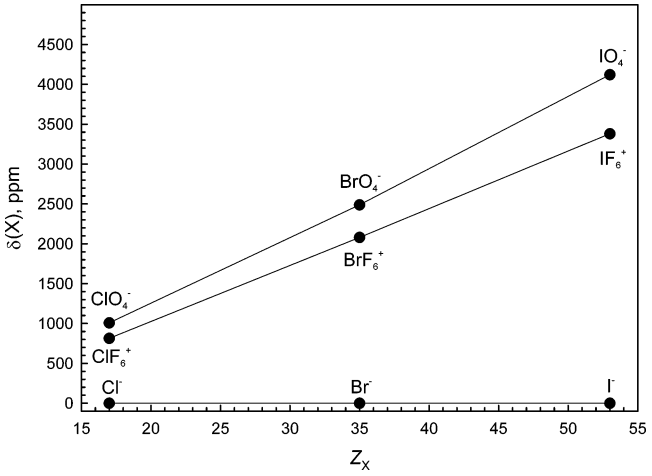

Figure 3. Plots of the halogen chemical shifts of XF_6^+, XO_4^-, and X^- ions (X = Cl, Br, I) versus atomic number, Z_X.

Table 5. Comparison of the Central Halogen Shielding Range Ratios and $\langle r^{-3}\rangle_p$ Ratios for ClF_6^+, BrF_6^+, and IF_6^+

central halogen			
X	Y	Δ_X/Δ_Y [a]	$\langle r^{-3}\rangle_{pX}/\langle r^{-3}\rangle_{pY}$ [b]
ClF_6^+	BrF_6^+	0.392	0.528
ClO_4^-	BrO_4^-	0.405[c]	
ClF_6^+	IF_6^+	0.241	0.398
ClO_4^-	IO_4^-	0.244[c]	
BrF_6^+	IF_6^+	0.615	0.753
BrO_4^-	IO_4^-	0.603[c]	

[a] The shielding ratios are defined as $\Delta_X/\Delta_Y = [\sigma(XF_6^+) - \sigma(X^-)]/[\sigma(YF_6^+) - \sigma(Y^-)]$ and $\Delta_X/\Delta_Y = [\sigma(XO_4^-) - \sigma(X^-)]/[\sigma(YO_4^-) - \sigma(Y^-)]$. [b] The values of $\langle r^{-3}\rangle_p$ are from ref 48. [c] The ratios of Δ_X/Δ_Y and $\langle r^{-3}\rangle_{pX}/\langle r^{-3}\rangle_{pY}$ for the XO_4^- (X = Cl, Br, I) anions were obtained from ref 49.

term is minimal, with the corresponding ratios of $\langle r^{-3}\rangle_{np}$ (Table 5). Although the magnitudes of both ratios differ slightly, they exhibit the same periodic trends. It is noteworthy that the chemical shift ratios for the XF_6^+ and XO_4^- ions[49] exceed the $\langle r^{-3}\rangle_{np}$ ratios, whereas the opposite is found when corresponding ratios are compared for compounds of the late group 14 (^{119}Sn and ^{207}Pb)[50] and group 16 (^{77}Se, ^{125}Te)[51] elements. The reversal within the XF_6^+ series may be a consequence of the high oxidation state (+7) of X, the highly ionic natures of their bonds, and neglect of the $\langle r^{-3}\rangle_{nd}$ contribution.[49]

The ^{127}I chemical shift of the IF_6^+ cation is deshielded relative to that of IF_7 (3095 ppm)[16] and is in accord with the deshieldings exemplified by the ^{77}Se, ^{125}Te, and ^{129}Xe chemical shifts of the fluoro cations of selenium,[52] tellurium,[53] and xenon[54,55] relative to those of their neutral parent fluorides[52,53,55,56] (also see details in ref 57). Nuclear deshielding upon cation formation is a consequence of the paramagnetic contribution to nuclear magnetic shielding (eq 13), which is negative and proportional to $\langle r^{-3}\rangle_{np}$, the electron imbalance terms, P_i and D_i, and the average excitation energy. Contraction of the valence p orbitals with increasing charge may be anticipated to be reflected in the X−F bond lengths. With few exceptions, the uncertainties in the average X−F bond lengths of the majority of cationic and neutral fluorospecies do not allow the correlation between deshielding of the central X nucleus and bond length contraction to be verified.[58−66] Significant bond length contractions do, however, occur for the XeF^+/XeF_2 and XeF_3^+/XeF_4 couples, and support the correlation (see ref 67 for details). In addition, a change in symmetry about the central nucleus is expected to result in a change in orbital mixing, when compared with the parent molecule, which leads to increased electron imbalance terms and nuclear deshielding. These interpretations are, at best, qualitative and ignore possible variations in the average excitation term, ΔE.

(c) Coupling Constants, $^1J(^mX-^{19}F)$, $^1K(X-F)$, and $^1K(X-F)_{RC}$ of the Group 14−18 Hexafluoro Species. The magnitudes of the isotropic coupling constants ($|^1J(^mX-^{19}F)|$) and reduced isotropic coupling constants ($|^1K(X-F)|$) obtained for the XF_6^+ cations in the present work are summarized in Table 4. The $|^1J(^mX-^{19}F)|$ coupling constants measured from the NMR spectra of the central halogen nuclei are in good agreement with those previously obtained from the ^{19}F NMR spectra $[ClF_6][AsF_6]$ ($|^1J(^{35}Cl-^{19}F)|$, 338−340; $|^1J(^{37}Cl-^{19}F)|$, 283−285.3 Hz),[8,9] $[ClF_6][SbF_6]$ ($|^1J(^{35}Cl-^{19}F)|$, 340; $|^1J(^{37}Cl-^{19}F)|$, 283 Hz),[8] $[ClF_6][PtF_6]$ ($|^1J(^{35}Cl-^{19}F)|$, 337; $|^1J(^{37}Cl-^{19}F)|$, 281 Hz),[4] $[BrF_6][AsF_6]$ ($|^1J(^{79}Br-^{19}F)|$, 1587; $|^1J(^{81}Br-^{19}F)|$, 1709 Hz),[6] $[BrF_6][Sb_2F_{11}]$ ($|^1J(^{79}Br-^{19}F)|$, 1575; $|^1J(^{81}Br-^{19}F)|$, 1697 Hz),[6] and $[IF_6][AsF_6]$ ($|^1J(^{127}I-^{19}F)|$, 2730 Hz)[15,16] in anhydrous HF solution. The value of $|^1J(^{127}I-^{19}F)|$ for $[IF_6][AsF_6]$ (2740 Hz),[16] in anhydrous HF, has also been determined from the ^{127}I NMR spectrum.[15] Although seldom extolled in the literature,

(49) Sanders, J. C. P. Ph.D. Thesis, University of Nottingham, Nottingham, U.K., 1986, p 82.
(50) Kennedy, J. D.; McFarlane, W.; Pyne, G. S. *J. Chem. Soc., Dalton Trans.* **1977**, 2332.
(51) McFarlane, H. C. E.; McFarlane, W. *J. Chem. Soc., Dalton Trans.* **1973**, 2416.
(52) Damerius, R.; Huppmann, P.; Lentz, D.; Seppelt, K. *J. Chem. Soc., Dalton Trans.* **1984**, 2821.
(53) Collins, M. J.; Schrobilgen, G. J. *Inorg. Chem.* **1985**, *24*, 2608.
(54) Birchall, T.; Myers, R. D.; de Waard, H.; Schrobilgen, G. J. *Inorg. Chem.* **1982**, *21*, 1068.
(55) Schrobilgen, G. J.; Holloway, J. H.; Granger, P.; Brevard, C. *Inorg. Chem.* **1978**, *17*, 980.
(56) Schumacher, G. A.; Schrobilgen, G. J. *Inorg. Chem.* **1984**, *23*, 2923.
(57) The ^{77}Se, ^{125}Te, and ^{129}Xe chemical shifts of SeF_3^+ (1135 ppm, SO_2-ClF solvent),[52] TeF_3^+ (671.2 ppm, SO_2 solvent),[53] XeF^+ (−574 ppm, SbF_5 solvent),[54,55] XeF_3^+ (595 ppm, SbF_5 solvent),[55] and XeF_5^+ (12.7 ppm, HF solvent)[55] are all significantly deshielded with respect to their parent fluorides; SeF_4 (1083 ppm, CH_3F solvent),[52] TeF_4 (606.6 ppm, SO_2 solvent),[53] XeF_2 (−2009 ppm, $CFCl_3$ solvent),[55] XeF_4 (202.9 ppm, $CFCl_3$ solvent),[56] and XeF_6 (−60.8 ppm, a tetramer in CF_2Cl_2/SO_2ClF solvent).[55]
(58) Edwards, A. J.; Jones, G. R. *J. Chem. Soc. A* **1970**, 1891.
(59) Edwards, A. J.; Taylor, P. *J. Chem. Soc., Dalton Trans.* **1973**, 2150.
(60) Burbank, R. D. *Acta Crystallogr.* **1962**, *15*, 1207.
(61) Bowater, I. C.; Brown, R. D.; Burden, F. R. *J. Mol. Spectrosc.* **1968**, *28*, 454.
(62) Edwards, A. J.; Hewaidy, F. I., *J. Chem. Soc. A* **1968**, 2977.
(63) Elliot, St. A.; Jenkins, H. D. B.; Schrobilgen, G. J.; Lehmann, J. F. Unpublished results.
(64) McKee, D. E.; Zalkin, A.; Bartlett, N. *Inorg. Chem.* **1973**, *12*, 1713.
(65) Reichman, S.; Schreiner, F. *J. Chem. Phys.* **1969**, *51*, 2355.
(66) Burns, J. H.; Agron, P. A.; Levy, H. A. *Science* **1963**, *139*, 1208.
(67) The differences between the bond lengths of the cation and the neutral species are not significant at the $\pm\sigma$ level for IF_6^+ (1.779(6) Å, $Sb_2F_{11}^-$ salt; this work), SeF_3^+ (1.73(4) Å, $Nb_2F_{11}^-$ salt),[58] and TeF_3^+ (1.84-(2) Å, $Nb_2F_{11}^-$ salt)[59] when compared with those of the neutral parent fluorides IF_7 (1.87(7) Å),[60] SeF_4 (1.72(5) Å),[61] and TeF_4 (1.86(6) Å).[62] Significant Xe−F bond length contractions occur for the XeF^+ (1.888-(4) Å, $Sb_2F_{11}^-$ salt)[63] and XeF_3^+ (weighted average: 1.87(5) Å, $Sb_2F_{11}^-$ salt)[64] when compared with those of the parent fluorides, XeF_2 1.9773(15) Å[65] and XeF_4 1.953(4) Å.[66]

J-couplings are more accurately determined from the NMR spectra of the high-spin quadrupolar nuclei than from the NMR spectrum of the spin-$^1/_2$ nucleus coupled to ^{m}X owing to the shorter relaxation times of ^{m}X relative to ^{19}F.[39,68] Thus, the $|^1J(^m\text{X}-^{19}\text{F})|$ coupling constants determined from the spectra of the central high-spin ^{m}X nuclides in the present work, and previously for $[IF_6][AsF_6]$[16] are somewhat larger than those obtained from the ^{19}F NMR spectra.

(i) Dominant Contributions to $^1J(^m\text{X}-^{19}\text{F})$. The magnitudes and signs of $^1J(^m\text{X}-^{19}\text{F})$ ($^m\text{X} = {}^{35}\text{Cl}$, ^{79}Br, ^{127}I) for the XF_6^+ cations have recently been calculated using relativistic density functional theory (the ZORA-DFT method).[69] The magnitudes of the calculated isotropic *J*-coupling constants, $^{35}ClF_6^+$ (344 Hz), $^{79}BrF_6^+$ (1398 Hz), and $^{127}IF_6^+$ (2793 Hz), are in good agreement with the experimental values (vide supra). The signs of the calculated coupling constants were found to be negative in each case and are in accord with a previous empirical prediction (vide infra) that the signs of $^1K(\text{X}-\text{F})$ for the isoelectronic hexafluoro species of groups 14−17 are all negative.[6]

Ramsey's nonrelativistic formalism[70] describes the indirect coupling of nuclear spins in terms of three coupling mechanisms, which contribute to the isotropic *J*-coupling: the Fermi-contact (FC) term and noncontact terms consisting of the spin−orbit (SO) mechanism, which is subdivided into diamagnetic (DSO) and paramagnetic (PSO) contributions, and the spin−dipolar (SD) contribution. The FC mechanism is customarily assumed to be the dominant coupling term; however, the remaining noncontact terms can also make significant contributions. For example, the PSO mechanism is dominant for XF (X = Cl, Br, I) and XeF^+.[69] Both noncontact terms are dependent on $\langle r^{-3}\rangle_{np}$, the expectation value of the inverse cube of the electron−nuclear distance of the valence p orbitals, which have a periodic dependence and are comparatively large for the halogens.[48]

The indirect nuclear spin−spin coupling tensors of the XF_6^+ cations calculated using the ZORA-DFT method[69] did not separate the FC and SD terms; however, the FC + SD contributions dominated the isotropic indirect spin−spin coupling. The PSO term was shown to be highly dependent upon the number of electron lone pairs on the central heavy atom and was minimal for the XF_6^+ cations, which displayed low PSO/(FC + SD) ratios for ClF_6^+ (14/86), BrF_6^+ (24/76), and IF_6^+ (18/82).[69] In the ensuing discussion, the relative roles of the FC term and of the noncontact terms, SD and PSO, are assessed, semiempirically, for the hexafluoro species of groups 14−17 by examining trends among their isotropic reduced coupling constants.

The present discussion of the FC contributions to the $^1J(^m\text{X}-^{19}\text{F})$ coupling constants of the XF_6^+ cations and isovalent species of groups 14−17 and rows 3−6 makes use of the formalism developed by Pople and Santry.[71] The FC term is given by eq 14, where all undefined symbols have their usual meanings and values, $|\Psi_{ns,\text{X}}(0)|^2$ and $|\Psi_{2s,\text{F}}(0)|^2$ are the s electron densities of the *n*s valence orbitals at the nuclei of the X and F atoms, and Π_{XF} is the mutual polarizability of the *n*s orbitals of X and F and is equivalent to the $P^2_{ns\text{X}/2s\text{F}}$ ($^3\Delta E)^{-1}$ terms in the formalism of McConnell,[72] where $P_{ns\text{X}/2s\text{F}}$ is the s bond order term and $^3\Delta E$ is an average triplet excitation energy. For closely related series, the magnitudes of the coupling constants are expected to be proportional to the s electron densities at the spin-coupled nuclei and to the square of the s bond order, $P^2_{ns\text{X}/2s\text{F}}$.

$$J(^m\text{X}-^{19}\text{F}) = -\frac{4\mu_o{\mu_B}^2}{9\pi}\gamma_X\gamma_F|\Psi_{ns,\text{X}}(0)|^2|\Psi_{2s,\text{F}}(0)|^2\Pi_{\text{XF}} \quad (14)$$

(ii) Periodic Trends in $^1K(\text{X}-\text{F})$. The spin−spin coupling constants of the XF_6^+ series are not directly comparable because $^1J(^m\text{X}-^{19}\text{F})$ is also proportional to the product of the gyromagnetic ratios of ^{m}X and ^{19}F. The reduced coupling constant, $K(\text{X}-\text{F})$ (eq 15), removes the nuclear dependence

$$K(\text{X}-\text{F}) = \frac{4\pi^2 J(^m\text{X}-^{19}\text{F})}{h\gamma_X\gamma_F} \quad (15)$$

of the spin−spin coupling by factoring out the gyromagnetic ratios of the spin-coupled nuclei,[73,74] allowing comparisons to be made among spin−spin coupling constants of different nuclides of the same element and nuclides of different elements. The γ-values are positive for the naturally occurring spin-active nuclides of groups 14, 16, and 17, but are negative for those of group 15. Thus, the sign of $^1K(\text{X}-\text{F})$ is also dependent on the group that X belongs to.

The substitution of eq 14 into eq 15 gives eq 16, which shows that $^1K(\text{X}-\text{F})$ is proportional to the products of $|\Psi_{ns,\text{X}}(0)|^2$ and Π_{XF} when it is dominated by the FC mechanism. The Π_{XF} and $|\Psi_{2s,\text{F}}(0)|^2$ terms, to a first approximation, may be treated as constants for the structurally related and isovalent group 14−17 hexafluoro species, so that plots of $^1K(\text{X}-\text{F})$ versus $|\Psi_{ns,\text{X}}(0)|^2$ are expected to yield linear relationships having slopes that are proportional to $|\Psi_{ns,\text{F}}(0)|^2\Pi_{\text{XF}}$. The s electron densities of the valence orbitals at the nuclei of the main-group elements have been calculated for their free atoms,[75] and can be used as estimates of $|\Psi_{ns,\text{X}}(0)|^2$ and $|\Psi_{2s,\text{F}}(0)|^2$ for the group 14−17 hexafluoro species assuming that bonding has a negligible effect on the valence s orbital electron densities at the spin-coupled nuclei. Relativistic corrections have been applied to $|\Psi_{ns,\text{X}}(0)|^2$ of the main-group elements of rows 4−6,[75] with the corrected values denoted by $|\Psi_{ns,\text{X}}(0)|^2_{\text{rel}}$, but have not been applied to the row 1−3 elements where relativistic effects are

$$K(^m\text{X}-^{19}\text{F}) = -\frac{16}{9}\pi\mu_o{\mu_B}^2|\Psi_{ns,\text{X}}(0)|^2|\Psi_{2s,\text{F}}(0)|^2\Pi_{\text{XF}} \quad (16)$$

(68) Chevalier, Y. *Magn. Reson. Chem.* **1986**, *24*, 404.
(69) Bryce, D. L.; Wasylishen, R. E. *Inorg. Chem.* **2002**, *41*, 3091.
(70) Ramsey, N. F. *Phys. Rev.* **1953**, *91*, 303.
(71) Pople, J. A.; Santry, D. P. *Mol. Phys.* **1964**, *8*, 1.
(72) McConnell, H. M. *J. Chem. Phys.* **1956**, *24*, 460.
(73) Mason, J. In *Multinuclear NMR*; Mason, J., Ed.; Plenum Press: New York, 1987; Appendix, pp 623−629.
(74) The values of the gyromagnetic ratios used in this study are ^{19}F (25.1815×10^7 rad s^{-1} T^{-1}), ^{35}Cl (2.6242×10^7 rad s^{-1} T^{-1}), ^{37}Cl (2.1844×10^7 rad s^{-1} T^{-1}), ^{79}Br (6.7256×10^7 rad s^{-1} T^{-1}), ^{81}Br (7.2498×10^7 rad s^{-1} T^{-1}), and ^{127}I (5.3896×10^7 rad s^{-1} T^{-1}) and were taken from ref 73.
(75) Pyykkö, P.; Wiesenfeld, L. *Mol. Phys.* **1981**, *43*, 557.

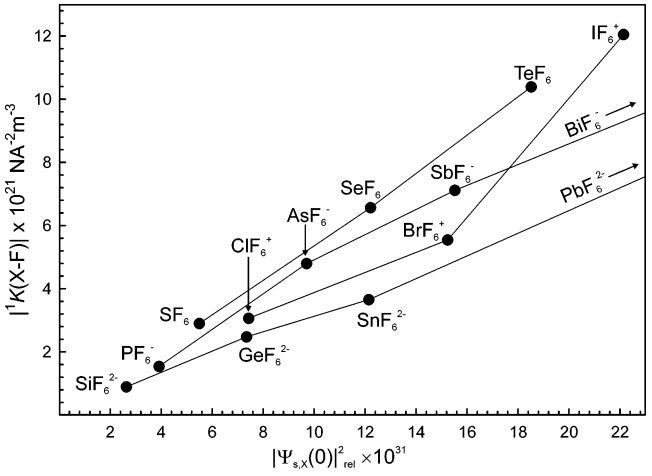

Figure 4. Plots of the reduced coupling constants, $|^1K(X-F)|$, of the XF_6^+, XF_6, XF_6^-, and XF_6^{2-} series versus $|\Psi_{ns,X}(0)|^2_{rel}$. The coordinates for the row 6 hexafluoro anions are as follows: BiF_6^- ($|^1K(X-F)|$, 20.60; $|\Psi_{ns,X}(0)|^2_{rel}$ 56.54) and PbF_6^{2-} ($|^1K(X-F)|$, 14.01; $|\Psi_{ns,X}(0)|^2_{rel}$, 40.99).

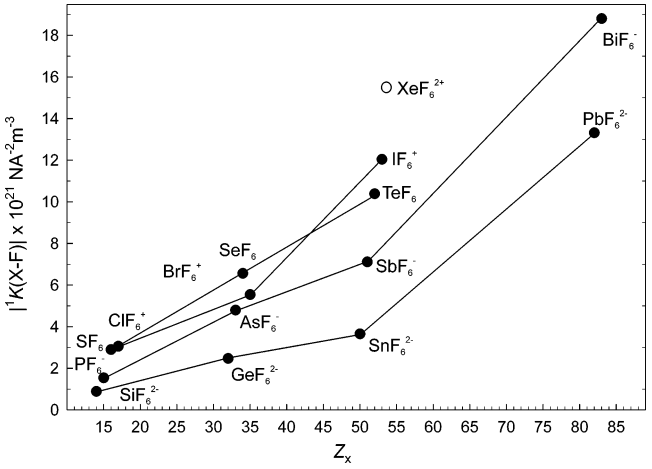

Figure 5. Plots of the reduced coupling constants, $|^1K(X-F)|$, versus atomic number, Z_X, for the isovalent group 14−17 hexafluoro species.

negligible. Relativistic effects for the heavier elements result in contraction of the valence s orbitals such that $|\Psi_{ns,X}(0)|^2_{rel}$ is invariably greater than $|\Psi_{ns,X}(0)|^2$. The relationship between $|^1K(X-F)|$ and $|\Psi_{ns,X}(0)|^2_{rel}$ for the group 14−17 hexafluoro species is shown in Figure 4. The correlations for groups 14−16 are nearly linear with positive slopes that intersect near the origin. Although the XF_6^+ cations exhibit a nonlinear relationship, with a line of best fit having a slope that is intermediate with respect to those of the group 14 and 15 species, the general observation that $|^1K(X-F)|$ increases with increasing $|\Psi_{ns,X}(0)|^2_{rel}$ and approaches zero as $|\Psi_{ns,X}(0)|^2_{rel}$ approaches zero is also consistent with the overall dominance of the FC term for these octahedral species and is consistent with the smaller PSO contributions that have been calculated for the XF_6^+ cations.[69]

The relationship between $|^1K(X-F)|^{1/2}$ and Z_X has been previously described for the isovalent hexafluorides of periods 14−17.[6] Similar trends are noted in the present work when $|^1K(X-F)|$ is plotted against Z_X (Figure 5), where the value of $|^1K(X-F)|$ increases, within each group, in a near-linear fashion with increasing Z_X for rows 3−4. The plots also increase, with positive slopes, from left to right across

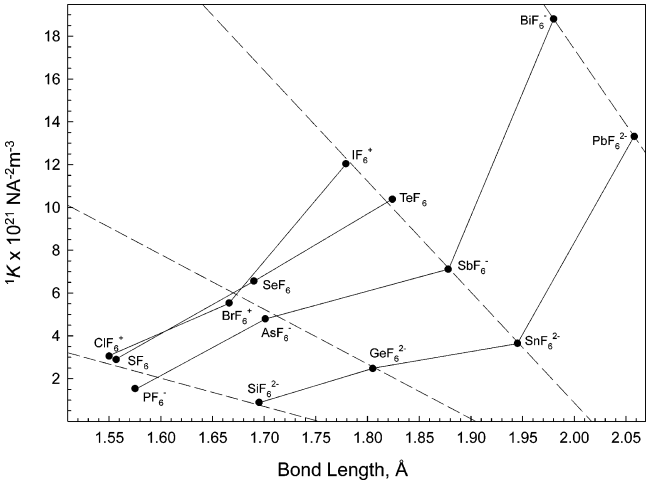

Figure 6. Plots of the reduced coupling constants, $|^1K(X-F)|$, of the isoelectronic group 14−17 hexafluoro species versus the average X−F bond length.

the periodic table within each isovalent series, intersecting near the origin. The increase in $|\Psi_{ns,X}(0)|^2_{rel}$ with increasing Z_X across each row is also an established trend,[76] and is reflected in plots of $|^1K(X-F)|$ versus Z_X; however, the halogen series deviates from the near-linear trends observed for groups 14, 15, and 16. The most notable deviations occur for ClF_6^+ and BrF_6^+, where the value of $|^1K(Cl-F)|$ for ClF_6^+ is similar to $|^1K(S-F)|$ of SF_6 and $|^1K(Br-F)|$ of BrF_6^+ is lower than $|^1K(Se-F)|$ of SeF_6. This anomaly may be attributable to the noncontact contributions identified in the previous theoretical study of the XF_6^+ cations, where the PSO terms accounted for 14% (ClF_6^+), 24% (BrF_6^+), and 18% (IF_6^+) of $|^1K(X-F)|$.[69] Although the anomalous behaviors of BrF_6^+ and, to a more limited extent, ClF_6^+ are noteworthy and may result from different relative contributions from the contact and noncontact terms, it is not possible to comment further on these anomalies in the absence of the PSO/(FC + SD) ratios for the hexafluoro species of groups 14−16.

A plot of $|^1K(X-F)|$ versus X−F bond length exhibits a positive slope within each group (Figure 6), but of greater interest is the relationship between $|^1K(X-F)|$ and the X−F bond lengths across each row. Plots of $|^1K(X-F)|$ for isoelectronic members of rows 3 and 4 versus their X−F bond lengths exhibit significant deviations from linearity when compared with the plot for the row 5 species. Although the PSO contribution is expected to be small when there are no electron lone pairs on the central atom,[69] it is clear from lines of best fit that $|^1K(X-F)|$ increases with decreasing bond length within each row, suggesting a dependence on $\langle r^{-3}\rangle_{np}$ and significant contributions from noncontact terms. The observed trends, however, are also consistent with $|\Psi_{ns,X}(0)|^2_{rel}$ and s bond order trends, which increase across each row and down each group, and provide significant contributions to the FC mechanism.

(iii) Absolute Signs of $^1J(^mX-^{19}F)$ and $^1K(X-F)$. The relative signs of the $^1K(X-F)$ coupling constants involving

(76) Jameson, C. J. In *Multinuclear NMR*; Mason, J., Ed.; Plenum Press: New York, 1987; Chapter 4, p 100.

main-group elements have been surveyed by Jameson,[77] but definitive assignments of the absolute signs for the majority of spin−spin couplings have not been made. On the basis of similar trends observed for $|^1K(X-F)|$, when plotted against Z_X, X−F bond length, and $|\Psi_{s,X}(0)|^2_{rel}$ for the hexafluoro species of groups 14−17 (Figures 4−6), and recent confirmation that the isotropic coupling constants of the XF_6^+ cations are negative,[69] it may be inferred that the signs of the reduced coupling constants of the hexafluoro species of groups 14−17 are all negative. In contrast, the γ-values of the group 15 nuclides are all negative, suggesting that the trends depicted in Figures 4−6 are preserved because the $^1J(^mX-^{19}F)$ couplings of PF_6^-, AsF_6^-, SbF_6^-, and BiF_6^- are positive.

The established trends among group 14−17 hexafluoro species also have implications relating to the signs of $^1J(^{129}Xe-^{19}F)$ and $^1J(^{131}Xe-^{19}F)$ for known xenon fluoride species and the hypothetical octahedral Xe(VIII) species, XeF_6^{2+}. Because ^{129}Xe ($I = {}^1/_2$) has a negative γ-value and ^{131}Xe ($I = {}^3/_2$) a positive value, $^1J(^{129}Xe-^{19}F)$ and $^1J(^{131}Xe-^{19}F)$ will have opposite signs. The previously discussed trends indicate that $^1K(Xe-F)$ is negative and, from the assumption that all $^1K(X-F)$ values in Figures 4−6 are negative, $^1J(^{129}Xe-^{19}F)$ for XeF_6^{2+}, which is isoelectronic with the row 5 hexafluoro species, is predicted to be positive with an estimated magnitude of 4800 ± 930 Hz. The predicted sign is also in accord with the relative signs predicted from plots of experimental ^{19}F chemical shifts versus $^1J(^{129}Xe-^{19}F)$ for the known Xe−F bonded derivatives of xenon.[78] The latter relationship indicates that all $^1J(^{129}Xe-^{19}F)$ couplings involving Xe(II) and Xe(IV) have negative signs whereas those of Xe(VI) have the smallest magnitudes and can have either negative or positive signs. The relationship assigns positive and negative signs to the axial and equatorial $^{129}Xe-^{19}F$ couplings, respectively, of the XeF_5^+ cation. These empirical relationships also predict a positive value for the $^1J(^{129}Xe-^{19}F)$ coupling of XeO_3F_2 (991−1015 Hz),[78] which is the only Xe(VIII) species for which a $^{129}Xe-^{19}F$ coupling constant has been determined. These empirical assignments of the signs of $^1J(^{129}Xe-^{19}F)$ have been recently supported by ZORA-DFT calculations,[69] which also assigned positive signs to the axial and equatorial $^1J(^{129}Xe-^{19}F)$ coupling constants of the unknown XeF_7^+ cation but did not consider either the XeF_6^{2+} cation or XeO_3F_2.

Computational Results. (a) Geometries. The energy-minimized structures of the ClF_6^+, BrF_6^+, and IF_6^+ cations have been calculated with O_h symmetry using the HF, MP2, and local density functional (LDF) methods (Table 6). The ClF_6^+, BrF_6^+, and IF_6^+ bond lengths calculated by the HF method provided the best agreement with the average experimental value. In the case of each XF_6^+ cation, the X−F bond lengths determined by MP2 and LDF methods were found to be similar, but were consistently longer than the experimental values.

Table 6. Comparison of the Experimental and Calculated Bond Lengths (Å) for ClF_6^+, BrF_6^+, and IF_6^+

cation[a]	expt (av)	HF	MP2	LDF
ClF_6^+	1.550(4)	1.547	1.623	1.612
BrF_6^+	1.666(11)	1.663	1.731	1.730
IF_6^+	1.779(6)	1.811	1.874	1.869

[a] The geometries of the XF_6^+ cations were optimized with O_h symmetries, and the DZVP basis set was used for each calculation.

(b) Vibrational Frequencies. The infrared and Raman frequencies of the ClF_6^+,[3−5,8−10] BrF_6^+,[6,9,11] and IF_6^+ [12−15] cations have been previously determined. These octahedral cations are expected to have 15 normal modes of vibration, $A_{1g} + E_g + F_{2g} + 2F_{1u} + F_{2u}$, where the $\nu_1(A_{1g})$, $\nu_2(E_g)$, and $\nu_5(F_{2g})$ modes are Raman active, the $\nu_3(F_{1u})$ and $\nu_4(F_{1u})$ modes are infrared active, and the $\nu_6(F_{2u})$ mode is both Raman and infrared inactive. The previously reported experimental frequencies and intensities of the ClF_6^+, BrF_6^+, and IF_6^+ cations are listed in Table 7, where they are compared with those calculated by HF, MP2, and LDF methods. The unscaled vibrational frequencies of the XF_6^+ cations were consistently overestimated by the HF calculations and underestimated by the MP2 and LDF calculations.

The inactive $\nu_6(F_{2u})$ mode of ClF_6^+ was previously assigned at 353 cm^{-1} on the basis of the first overtone of $\nu_6(F_{2u})$ ($A_{1g} + E_g + F_{2g}$) at 706 cm^{-1} in the infrared spectrum[8] and is bracketed by the calculated frequencies (HF, 383 cm^{-1}; MP2, 308 cm^{-1}; LDF, 296 cm^{-1}). The $\nu_6(F_{2u})$ modes of BrF_6^+ and IF_6^+ have never been directly or indirectly observed; however, the calculations predict that their frequencies lie between 231 and 306 cm^{-1} and between 179 and 234 cm^{-1}, respectively.

In contrast with the ClF_6^+ cation, where $\nu_1(A_{1g})$ is at higher frequency than $\nu_2(E_g)$, the frequency order of these vibrational modes is reversed for BrF_6^+ ($\nu_1(A_{1g})$, 658 cm^{-1}; $\nu_2(E_g)$, 668 cm^{-1}) and IF_6^+($\nu_1(A_{1g})$, 708 cm^{-1}; $\nu_2(E_g)$, 732 cm^{-1}). The frequency orders of these bands are correctly predicted by the HF and MP2 calculations, but not by the LDF calculations, whereas the frequency orders of the remaining bands are correctly predicted by the three methods.

The calculated infrared and Raman intensities for the XF_6^+ cations are in semiquantitative agreement with the relative experimental intensities. Although the experimental absolute extinction coefficients of the infrared-active $\nu_3(F_{1u})$ and $\nu_4(F_{1u})$ bands of the XF_6^+ cations have not been determined, it is clear that the experimental transition moment of $\nu_3(F_{1u})$ is greater than that of $\nu_4(F_{1u})$. The experimental intensities are consistent with the intensities calculated by HF, MP2, and LDF methods, which provided $\nu_3(F_{1u})$:$\nu_4(F_{1u})$ intensity ratios of 9.0, 22.2, and 16.1 for ClF_6^+, 2.3, 3.7, and 4.0 for BrF_6^+, and 1.5, 2.0, and 4.0 for IF_6^+. The experimental Raman intensity of $\nu_1(A_{1g})$ is invariably greater than those of $\nu_2(E_g)$ and $\nu_5(F_{2g})$, and this trend is reproduced by the calculated intensities.

(c) Natural Bond Orbital (NBO) Analyses. The atomic charges and Mayer bond orders calculated for the XF_6^+ cations using the energy-minimized geometries determined from HF, MP2, and LDF calculations are summarized in

(77) Jameson, C. J. In *Multinuclear NMR*; Mason, J., Ed.; Plenum Press: New York, 1987; Chapter 4, p 92.
(78) Gerken, M.; Schrobilgen, G. J. *Coord. Chem. Rev.* 2**000**, *197*, 335.

Table 7. Comparison of Experimental and Calculated Vibrational Frequencies for XF_6^+ (X = Cl, Br, I)

assignment (O_h)		description[a]	expt[b,c]	HF[d]	MP2[d]	LDF[d]
ClF_6^+	$\nu_1(A_{1g})$	$\nu_{sym\ in\ phase}$	688 (100)	746 (33) [0]	599 (22) [0]	628 (31) [0]
	$\nu_2(E_g)$	$\nu_{sym\ out\ of\ phase}$	631 (27)	703 (26) [0]	556 (14) [0]	565 (16) [0]
	$\nu_3(F_{1u})$	ν_{asym}	890 [ms]	1017 (0) [1002]	804 (0) [867]	840 (0) [867]
	$\nu_4(F_{1u})$	$\delta_{umbrella}$	590 [m]	631 (0) [111]	518 (0) [39]	506 (0) [54]
	$\nu_5(F_{2g})$	$\delta_{scissor}$	517 (40)	550 (8) [0]	452 (10) [0]	440 (10) [0]
	$\nu_6(F_{2u})$	δ_{pucker}	353	383 (0) [0]	308 (0) [0]	296 (0) [0]
BrF_6^+	$\nu_1(A_{1g})$	$\nu_{sym\ in\ phase}$	658 (100)	739 (41) [0]	616 (24) [0]	623 (36) [0]
	$\nu_2(E_g)$	$\nu_{sym\ out\ of\ phase}$	668 (28)	746 (26) [0]	622 (7) [0]	614 (17) [0]
	$\nu_3(F_{1u})$	ν_{asym}	775 [ms]	885 (0) [420]	733 (0) [396]	736 (0) [363]
	$\nu_4(F_{1u})$	$\delta_{umbrella}$	427, 433 [m]	472 (0) [183]	400 (0) [108]	377 (0) [90]
	$\nu_5(F_{2g})$	$\delta_{scissor}$	405 (34)	435 (10) [0]	365 (11) [0]	345 (11) [0]
	$\nu_6(F_{2u})$	δ_{pucker}		306 (0) [0]	248 (0) [0]	231 (0) [0]
IF_6^+	$\nu_1(A_{1g})$	$\nu_{sym\ in\ phase}$	708 (100)	806 (39) [0]	622 (31) [0]	623 (39) [0]
	$\nu_2(E_g)$	$\nu_{sym\ out\ of\ phase}$	732 (20)	811 (19) [0]	651 (12) [0]	614 (15) [0]
	$\nu_3(F_{1u})$	ν_{asym}	797, 790 [ms]	892 (0) [357]	719 (0) [276]	736 (0) [363]
	$\nu_4(F_{1u})$	$\delta_{umbrella}$	343 [m]	378 (0) [231]	301 (0) [141]	377 (0) [90]
	$\nu_5(F_{2g})$	$\delta_{scissor}$	340 (40)	366 (9) [0]	278 (12) [0]	344 (11) [0]
	$\nu_6(F_{2u})$	δ_{pucker}		234 (0) [0]	179 (0) [0]	231 (0) [0]

[a] Abbreviations denote symmetric (sym), asymmetric (asym), medium (m), and medium strong (ms). [b] The observed Raman and infrared intensities are relative values and are given in parentheses and brackets, respectively. [c] Experimental vibrational frequencies and intensities are taken from ref 8 for $[ClF_6][AsF_6]$, from ref 6 (Raman frequencies) and ref 11 (infrared frequencies) for $[BrF_6][AsF_6]$, and from ref 12 for $[IF_6][AsF_6]$. [d] The calculated Raman and infrared intensities are given in parentheses and square brackets, respectively, and have units of and Å^4 amu^{-1} and km mol^{-1}, respectively.

Table 8. Atomic Charges, Valencies, and Mayer Bond Orders for the XF_6^+ (X = Cl, Br, I) Cations

		HF	MP2	LDF	ELF[a]
		Atomic Charges and Valencies[b]			
ClF_6^+	Cl	2.91 (3.10)	2.60 (2.72)	2.51 (2.93)	3.07
	F	−0.32 (0.37)	−0.27 (0.32)	−0.25 (0.36)	−0.34
BrF_6^+	Br	3.35 (3.11)	3.03 (2.86)	2.86 (2.95)	3.30
	F	−0.39 (0.40)	−0.34 (0.37)	−0.31 (0.39)	−0.38
IF_6^+	I	4.14 (2.91)	3.73 (2.78)	3.50 (2.85)	4.63
	F	−0.52 (0.40)	−0.46 (0.40)	−0.42 (0.40)	−0.60
		Bond Orders			
ClF_6^+	Cl−F	0.517	0.454	0.488	
	F···F_{cis}	−0.039	−0.034	−0.034	
	F···F_{trans}	0.008	0.004	0.004	
BrF_6^+	Br−F	0.519	0.477	0.492	
	F···F	−0.031	−0.026	−0.027	
	F···F_{trans}	0.003	0.001	0.001	
IF_6^+	I−F	0.485	0.464	0.475	
	F···F_{cis}	−0.022	−0.018	−0.019	
	F···F_{trans}	0.001	0.000	0.000	

[a] From the TopMod electron populations. [b] Valencies are given in parentheses.

Table 8. The calculated charges on the central halogen atoms are significantly less than +7, and those on the fluorine ligands are accordingly more positive than the −1 charge expected for purely ionic structures. The atomic charge distributions are consistent with the polarities of the X−F bonds based on the electronegativities[79] of fluorine (4.10), chlorine (2.83), bromine (2.74), and iodine (2.21), with the ionic character of the X−F bond increasing with atomic number of the central halogen.

The X−F Mayer bond orders calculated for ClF_6^+ (0.454 to 0.517), BrF_6^+ (0.477 to 0.519), and IF_6^+ (0.464 to 0.485) are comparable at a given level of theory and exhibit a minimal dependence on the computational method. The Mayer bond orders between *cis*-fluorine atom pairs are negative, decreasing in magnitude down the group as the size of the central halogen atom increases, i.e., ClF_6^+ (−0.034 to −0.039) > BrF_6^+ (−0.026 to −0.031) > IF_6^+ (−0.018 to −0.022), reflecting the reduction in F···F repulsions as the size of the central atom increases.

(d) Electron Localization Functions. The starting point of the Silvi−Savin approach to chemical bonding,[80] which is based on a topological analysis of the gradient field of the electron localization function (ELF), $\eta(r)$, is the single determinant of the HF wave functions comprising the entire set of occupied molecular orbitals obtained from a prior electronic structure calculation. Use of the complete MO set gives more realistic approximations of the total electron density than treatments based on forcing electron pairs into single molecular orbitals. In fact, single MO wave functions are intermediate results, which are optimized during the LCAO-SCF-HF procedure, as they are a part of the Fock operator.

The ELF calculations in the present work were completed using the HF method. The basin populations (N_i), relative fluctuations (λ), and contribution analyses (%) for the XF_6^+ cations are summarized in Table 9 (see Table S1 for more information). The ELF calculations identified core basins on the halogens, $C(X_i)$, the valence lone pair basins, $V_n(X_i)$, and the bond pair basins, $V(X,F_i)$, which are illustrated by the isosurfaces for each cation in Figure 7.

The lobes show high electron densities concentrated on the fluorine atoms. The core basin populations of chlorine (9.98), bromine (27.55), and iodine (45.70) are close to the expected electron counts of 10, 28, and 46, respectively, and the low λ values (Cl, 0.06; Br, 0.04; I, 0.03) indicate a high degree of electron localization for these basins with negligible interaction with the bonding basins. Similarly, the fluorine core basin populations in ClF_6^+ (2.07), BrF_6^+ (1.95), and IF_6^+ (2.07) are close to the expected value of 2; however, these basins are significantly more delocalized (λ, 0.22−0.23). The greater degrees of delocalization for the fluorine

(79) Allred, A. L.; Rochow, E. G. *J. Inorg. Nucl. Chem.* **1958**, *5*, 264.

(80) Silvi, B.; Savin, A. *Nature* **1994**, *371*, 683.

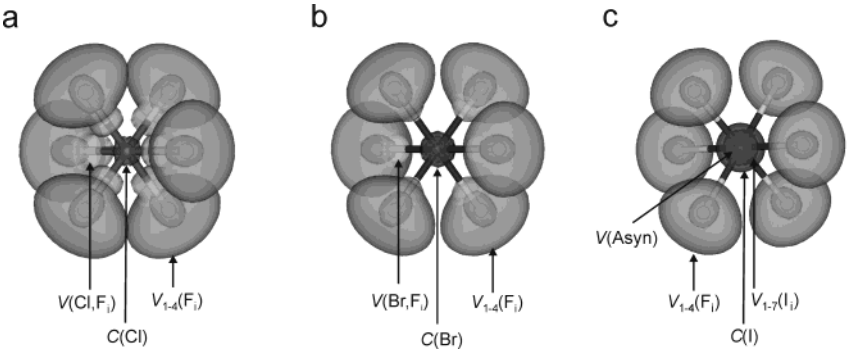

Figure 7. The ELF isosurface plots (0.67 contour) calculated at the HF/DZVP level for (a) ClF_6^+, (b) BrF_6^+, and (c) IF_6^+; symbol definitions are given in Table 9.

Table 9. Symmetry Averaged ELF Basin Separation Values (f_{sep}), Basin Volumes (V), Basin Populations (N_i), Relative Fluctuations (λ), and Contributions (%) of Other Basins to the Variances ($\sigma^2(N_i)$) for XF_6^+ (X = Cl, Br, I)[a]

basin[b]	N_i [e][b]	λ[c]	contribution analysis (%)[d]
ClF_6^+			
C(Cl)	9.98	0.06	13% each V(Cl,F$_j$)
C(F$_j$)	2.07	0.22	19%V_1(F$_j$); 22%V_2(F$_j$); 24%V_3(F$_j$); 27%V_4(F$_j$)
V_1(F$_j$)	1.38	0.62	10%C(F$_j$); 29%V_2(F$_j$); 28%V_3(F$_j$); 14%V_4(F$_j$); 11%V(Cl,F$_j$)
V_2(F$_j$)	1.61	0.58	10%C(F$_j$); 20%V_1(F$_j$); 24%V_3(F$_j$); 24%V_4(F$_j$); 12%V(Cl,F$_j$)
V_3(F$_j$)	1.61	0.58	10%C(F$_j$); 21%V_1(F$_j$); 22%V_2(F$_j$); 25%V_4(F$_j$); 11%V(Cl,F$_j$)
V_4(F$_j$)	1.93	0.54	12%C(F$_j$); 22%V_1(F$_j$); 22%V_2(F$_j$); 24%V_4(F$_j$); 13%V(Cl,F$_j$)
V(Cl,F$_j$)	1.25	0.71	11%V_1(F$_j$); 13%V_2(F$_j$); 13%V_3(F$_j$); 15%V_3(F$_j$)
BrF_6^+			
C(Br)	27.55	0.04	15% each V(Br,F$_j$)
C(F$_j$)	1.95	0.23	16%V_1(F$_j$); 18%V_2(F$_j$); 25%V_3(F$_j$); 27%V_4(F$_j$)
V_1(F$_j$)	1.39	0.62	19%V_2(F$_j$); 30%V_3(F$_j$); 24%V_4(F$_j$); 10%V(Br,F$_j$)
V_2(F$_j$)	1.55	0.60	15%V_1(F$_j$); 21%V_3(F$_j$); 33%V_4(F$_j$)
V_3(F$_j$)	1.84	0.56	14%C(F$_j$); 23%V_1(F$_j$); 19%V_2(F$_j$); 25%V_4(F$_j$); 11%V(Br,F$_j$)
V_4(F$_j$)	2.20	0.53	13%C(F$_j$); 18%V_1(F$_j$); 26%V_2(F$_j$); 23%V_4(F$_j$); 11%V(Br,F$_j$)
V(Br,F$_j$)	1.13	0.77	19%C(Br); 13%V_1(F$_j$); 11%V_2(F$_j$); 13%V_3(F$_j$); 15%V_4(F$_j$)
IF_6^+			
C(I)	45.70	0.03	
C(F$_j$)	2.07	0.22	21%V_1(F$_j$); 27%V_2(F$_j$); 30%V_3(F$_j$); 20%V(I,F$_j$)
V_{1-7}(I)	0.03	0.99	34%C(I)
V_1(F$_j$)	1.63	0.62	20%V_2(F$_j$); 31%V_3(F$_j$); 25%V_4(F$_j$)
V_2(F$_j$)	1.80	0.60	19%V_1(F$_j$); 29%V_3(F$_j$); 30%V_4(F$_j$)
V_3(F$_j$)	2.22	0.57	11%C(F$_j$); 25%V_1(F$_j$); 25%V_2(F$_j$); 25%V_4(F$_j$)
V_4(F$_j$)	2.28	0.55	11%C(F$_j$); 22%V_1(F$_j$); 26%V_2(F$_j$); 27%V_3(F$_j$)
V(Asyn)	0.02	0.99	

[a] All calculations were performed using the HF/DZVP method. [b] N_i is the basin population (e). Indices: i the basin in question, j = 1−6. [c] λ is the relative fluctuation of the basin population. [d] The total contribution of other basins to N_i is defined as the variance, $\sigma^2(N_i)$, with each indicated basin giving its percent contribution. Contributions less than 10% are not given.

core basins are attributed to contributions from the fluorine lone pair basins (ClF_6^+, 19−27%; BrF_6^+, 16−27%; IF_6^+, 20−30%), which vary from 0.45 to 0.46 electron. Each fluorine atom was found to have four lone pair basins with electron population ranges of 1.38 to 1.93, 1.39 to 2.20, and 1.63 to 2.28 for ClF_6^+, BrF_6^+, and IF_6^+, respectively. These four basins, which are indicative of high fluoride ion character, are highly delocalized with respect to each other (λ, 0.53−0.62), resulting in the continuous nature of these lobes as depicted in Figure 7.

The average bonding basin populations are 1.25 and 1.13 for ClF_6^+ and BrF_6^+, respectively. The bonding basins of ClF_6^+ and BrF_6^+ are highly delocalized (λ, 0.71−0.77), with the delocalization being attributed to the lone pair basins of the fluorine atoms and not to the core basins of the central halogen. As a result, the bonding electrons are more closely associated with the fluorine atoms (Figure 7). In contrast with the lighter halogen analogues, IF_6^+ does not have a bonding basin. It is therefore reasonable to conclude that the bonding in IF_6^+ is the most ionic of the XF_6^+ cations.

The ELF charges on Cl (3.07), Br (3.30), and I (4.63) and on the fluorine atoms of ClF_6^+ (−0.34), BrF_6^+ (−0.38), and IF_6^+ (−0.60) are comparable to those obtained from the NBO analyses (vide supra), with the magnitudes of the charge differences between the central halogen atoms and the fluorine ligands increasing upon descending group 17. The increasing ionic characters of the X−F bonds are also reflected in their declining valence shell occupancies of Cl (3.94), Br (3.70), and I (2.37).

Bonding and Structural Trends Among the XF_6^+ Cations and Related Fluoride Species. (a) Nature of X−F Bonding in the XF_6^+ Cations. The octahedral symmetry allows a simple view of the σ bonding. The six symmetry-adapted fluorine orbitals contributing to the bonding combine with available orbitals on the central X atom.[81] Four symmetry-adapted fluorine orbitals combine with the central atom s and p orbitals to generate four filled bonding orbitals (one A_{lg} and three T_{lu}). The remaining two filled fluorine-ligand orbitals are nonbonding with E_g symmetry, and are fluorine only in character if there is no central atom d orbital participation. This bonding model ensures that the X−F bonds will have appreciable polarities. Participation of d orbitals would lower bond polarities and enhance the bond energies.

The failure of the XF_6^+ cations to fulfill the basic requirements for three center bonds (a coordination number in excess of four and the presence of a sterically active, free valence electron pair on the central atom)[82,83] also implies

(81) Kutzelnigg, W. *Angew. Chem., Int. Ed. Engl.* **1984**, *23*, 272; *Angew. Chem.* **1984**, *96*, 262.
(82) Christe, K. O. In *XXIVth International Congress of Pure and Applied Chemistry*; Butterworth: London, 1974; Vol. 4, p 115.

that their bonding is best described in terms of covalent two center bonds with strong ionic contributions. This model is consistent with the NBO and ELF analyses, which predict covalent bond orders of approximately $^1/_2$ and increasing bond polarities as the electronegativity of the central atom decreases. The combination of these bonding contributions leads to X−F bond lengths that are among the shortest known for the neutral and charged binary halogen fluorides. A description of the bonding orbitals of the central atom is ambiguous and a moot issue because bonding is not an observable quantity; only bonding distances and electron density are amenable to observation and direct measurements. For solely didactic reasons, the octahedral geometries of the XF_6^+ cations and the high covalencies of their bonds could be explained either by the classic sp^3d^2 hybridization model of the halogen orbitals[84] or by a more preferred model, which uses the s and three p orbitals of the central atom and avoids the use of d orbitals for the description of bonding in main-group compounds.[81]

(b) Assessment of Ligand Close Packing among the Isovalent Hexafluoro Species of Groups 14−17. Bond length contraction with increasing central halogen oxidation state is likely offset by increases in the magnitudes of the intramolecular F···F repulsive interactions when the halogen atom is in a high oxidation state (+5 or +7), has a high coordination number, and has a net positive charge. Significant ligand−ligand repulsions, which are a consequence of the smaller size of the central halogen atom, can account for the inability of chlorine and bromine to exhibit coordination numbers that exceed six. This hypothesis is supported by the negative Mayer bond orders between *cis*-fluorine atoms, which decrease in the order ClF_6^+ (−0.034) > BrF_6^+ (−0.027) > IF_6^+ (−0.019), and the increase in the average experimental intra-ionic F···F distances, ClF_6^+ (2.192(5) Å) < BrF_6^+ (2.356(11) Å) < IF_6^+ (2.516(17) Å). The present experimental findings are in accord with the views of Robinson and Gillespie,[85] who have recently investigated the role of ligand close packing (LCP) in octahedral main-group fluorides of rows 3, 4, and 5 and concluded from the experimental intra-ionic F···F distances[86] that the fluorine ligands of ClF_6^+ are close packed whereas those of BrF_6^+ and IF_6^+ are not. They go on to point out that although the F ligands of row 4 species, such as BrF_6^+, are not close packed because of the larger sizes of row 4 atoms, the central atoms are not large enough to accommodate more than six ligands, contrasting with the row 5 elements which can accommodate as many as seven or eight small ligand atoms.

Comparisons among the isovalent main-group hexafluoro species, XF_6^+ (X = Cl, Br, I), XF_6 (X = S, Se, Te), XF_6^- (X = P, As, Sb), and XF_6^{2-} (X = Si, Ge, Sn), also reveal several relationships among their net charges, X−F bond lengths (Figure 8), and F···F contact distances. With the exception of the dianions, SiF_6^{2-} (1.695(5)/*2.40* Å)[87] and GeF_6^{2-} (1.80(4)/*2.55* Å),[88] the X−F bond lengths and F···F contact distances (values in italics) do not differ significantly among the row 3 (ClF_6^+, 1.550(4)/*2.19* Å; SF_6, 1.5568(6)/*2.202* Å;[89] PF_6^- 1.58(1)/*2.23* Å[90]) and row 4 (BrF_6^+, 1.666-(11)/*2.36* Å; SeF_6, 1.69(1)/*2.39* Å;[91] AsF_6^- 1.70(2)/*2.40* Å[92]) hexafluoro species. The absence of a significant dependence of the X−F bond lengths on net charge suggests that the bond contraction expected with increasing oxidation state along each row is counterbalanced by F···F ligand−ligand interactions in rows 3 and 4. Repulsive interactions of this kind are not surprising considering that the F···F contacts are significantly less than twice the sum of the van der Waals radius of fluorine (2.70,[20] 2.94 Å[21]). This is not the case for row 5 and 6 hexafluoro species, where the X−F bond lengths clearly exhibit a contraction as the net charge becomes more positive (SnF_6^{2-}, 1.945(2)/*2.75* Å;[93] SbF_6^-, 1.878(4)/*2.66* Å;[92] TeF_6, 1.824(4)/*2.58* Å;[94] IF_6^+, 1.779(6)/*2.52* Å and PbF_6^{2-}, 2.058(4)/*2.91* Å;[95] BiF_6^-, 1.98(5)/*2.80* Å[96]) and the F···F contact distances approach the van der Waals sum for the anionic species. The reduced ligand−ligand interactions among the row 5 and 6 hexafluoro species are also consistent with the ability of their central atoms to exhibit coordination numbers as high as seven (IF_7,[97] TeF_7^-,[98] SbF_7^{2-} [99]) and eight (TeF_8^{2-},[98] IF_8^{2-} [100]).

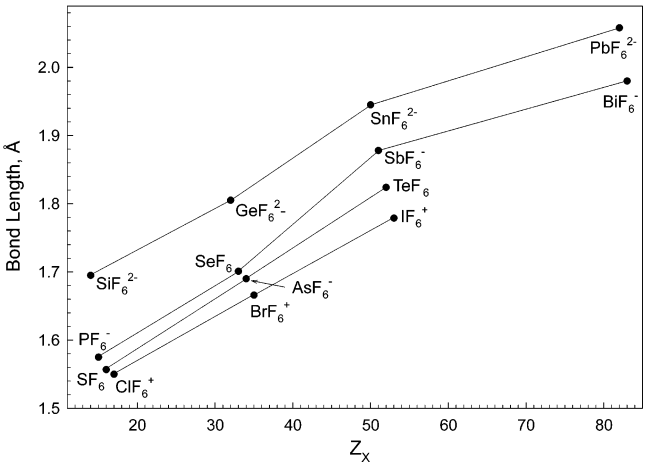

Figure 8. Plots of the average X−F bond lengths of the isovalent group 14−17 hexafluorides versus atomic number, Z_X.

(83) Christe, K. O.; Schack, C. J. *Adv. Inorg. Chem. Radiochem.* **1976**, *18*, 319.
(84) Holleman, A. F.; Wiberg, E. In *Inorganic Chemistry*; Wiberg, N., Aylett, B. J., Eds.; Academic Press: San Diego, 2001; pp 331−337.
(85) Robinson, E. A.; Gillespie, R. J. *Inorg. Chem.* **2003**, *42*, 3865.
(86) The Br−F bond length (1.55Å) and intraionic F···F contact distance (2.19 Å) cited for the BrF_6^+ cation in Table 4 of ref 85 are erroneous; the values should be 1.666(11) and 2.356(11) Å, respectively.
(87) Zalkin, A.; Forrester, J. D.; Templeton, D. H. *Acta Crystallogr.* **1964**, *17*, 1408.
(88) Popov, D. Y.; Kavun, V. Y.; Gerasimenko, A. V.; Sergienko, V. I.; Antokhina, T. F. *Russ. J. Inorg. Chem.* **1999**, *44*, 97; *Zh. Neorg. Khim.* **1999**, *44*, 103.
(89) Ischenko, A.; Ewbank, J. D.; Schäfer, L. *J. Phys. Chem.* **1994**, *98*, 4287.
(90) Wang, Y.; Calvert, L. D.; Brownstein, S. K. *Acta Crystallogr., Sect. B* **1980**, *36*, 1523.
(91) Ewing, V. C.; Sutton, L. E. *Trans. Faraday Soc.* **1963**, *59*, 1241.
(92) Lehmann, J. F.; Dixon, D. A.; Schrobilgen, G. J. *Inorg. Chem.* **2001**, *40*, 3002.
(93) Benghalem, A.; Leblanc, M.; Calage, Y. *Acta Crystallogr., Sect. C* **1990**, *46*, 2453.
(94) Seip, H. M.; Stølevik, R. *Acta Chem. Scand.* **1966**, *20*, 1543.
(95) Brock, D. S.; Mercier, H. P. A.; Schrobilgen, G. J. Unpublished results.
(96) Lucier, G.; Münzenberg, J.; Casteel, W. J.; Bartlett, N. *Inorg. Chem.* **1995**, *34*, 2692.
(97) Ruff, O.; Keim, R. *Z. Anorg. Chem.* **1931**, *201*, 245.
(98) Selig, H.; Sarig, S.; Abramowitz, S. *Inorg. Chem.* **1974**, *13*, 1508.

Conclusion

The X-ray crystal structures of the XF_6^+ (X = Cl, Br, I) cations have been determined for the first time as their isomorphous $Sb_2F_{11}^-$ salts. The XF_6^+ cations display among the shortest X−F bond lengths known for the neutral and charged binary halogen fluorides. The vibrational frequencies and intensities of the XF_6^+ cations, derived from the electronic structure calculations, confirm the previous assignments of their infrared and Raman spectra.

The ^{35,37}Cl, ^{79,81}Br, and ^{127}I NMR spectra of the ClF_6^+, BrF_6^+, and IF_6^+ cations and their T_1-relaxation times reflect the octahedral geometries of these cations in HF solution. The central halogen chemical shifts of XO_4^- and XF_6^+ increase significantly when descending the halogen group, reflecting the dominance of the paramagnetic shielding terms for the heavier nuclei, paralleling the larger values of $\langle r^{-3}\rangle_{np}$ associated with these elements. Trends in isotropic reduced coupling constants, $|^1K(X-F)|$, with $|\Psi_{ns,X}(0)|^2$ and Z_X for the row 3−5 hexafluoro species have near-linear relationships across each row that are consistent with the dominant role of the Fermi contact spin−spin coupling mechanism. The anomalous behaviors of BrF_6^+ and, to a lesser extent, ClF_6^+ within these relationships may result from different relative contributions from the contact and noncontact terms. The $|^1K(X-F)|$ couplings increase linearly across a row from left to right as the X−F bond length decreases, with the best correlation being observed for row 5 hexafluoro species where intraionic F···F repulsions are minimized. From the similar behaviors of $|^1K(X-F)|$ with respect to $|\Psi_{ns,X}(0)|^2$, Z_X and the X−F bond lengths of the group 14−17 hexafluoro species of rows 3−5, it is inferred that their $^1K(X-F)$ coupling constants have the same sign. Furthermore, the recently established negative signs for $^1J(^mX-^{19}F)$ of the XF_6^+ cations also imply that the signs of $^1J(^mX-^{19}F)$ are negative for the group 14 and 16 hexafluoro species, but positive for the group 15 analogues and for the presently unknown $^{129}XeF_6^{2+}$ cation.

The experimental and calculated bond length trends among the XF_6^+ cations are governed by the degree of covalent character in their semi-ionic bonds, which decreases as the electronegativity of X decreases. The magnitudes of the calculated atomic charges on the central halogen atoms and fluorine atoms, which increase upon descending group 17, reflect this trend. The X−F Mayer bond orders were similar for the ClF_6^+, BrF_6^+, and IF_6^+ cations; however, intra-ionic F···F bond orders were found to become less negative down the group, reflecting the ability of iodine to achieve coordination numbers greater than six. The ELF approach has provided a means to visualize the bonding electron density and relative ionicities of the X−F bonds in the XF_6^+ cations. The positions of the ELF bonding basins along the X−F bond paths are consistent with single, highly polar X−F bonds that also parallel the effective electronegativities of the halogens, with X−F bond ionicities increasing in the order $ClF_6^+ < BrF_6^+ < IF_6^+$.

Experimental Section

CAUTION! Anhydrous HF must be handled using appropriate protective gear with immediate access to proper treatment procedures[101−103] in the event of contact with liquid HF, HF vapor, or HF-containing solutions. Krypton difluoride and the salts of KrF^+, $Kr_2F_3^+$, ClF_6^+, BrF_6^+, and IF_6^+ are extremely strong oxidants and react vigorously to explosively with water, organic materials, and other oxidizable materials. Extreme caution is to be exercised during the handling and disposal of these species to avoid violent detonations.

Apparatus and Materials. Volatile materials were handled in vacuum lines constructed of stainless steel, nickel, and $^1/_4$-in.-o.d. FEP fluoroplastic tubing, and nonvolatile materials were transferred in the dry atmosphere of a drybox as previously described.[104]

(a) General Reagents. Krypton difluoride,[92] AsF_5,[105] ClF_5,[106] and IF_7[107] were prepared and purified according to literature methods. The oxidizing agent $[KrF][AsF_6]$ was prepared by the literature method,[108] by reaction of KrF_2 with AsF_5 in anhydrous HF, and its purity was monitored by low-temperature Raman spectroscopy. Solutions of SbF_5 in anhydrous HF were prepared by the direct fluorination of freshly sublimed SbF_3 (Aldrich, 98%), as previously described.[109] Antimony pentafluoride (Ozark Mahoning),[109] used in the preparation of $[IF_6][Sb_3F_{16}]$, and BrF_5 (Ozark Mahoning)[108] were purified as previously described. Anhydrous HF was purified as previously described[110] and stored over BiF_5. Ultrahigh purity (UHP) argon (Air Liquid; certified 99.999%, <2 ppm O_2, <3 ppm H_2O) was used without further purification.

(b) $[ClF_6][AsF_6]$ and $[BrF_6][AsF_6]$. The salts $[ClF_6][AsF_6]$[8] and $[BrF_6][AsF_6]$[6] were prepared in FEP reaction vessels equipped with stainless steel valves by allowing the oxidant $[KrF][AsF_6]$ (0.5 g) to react with approximately 0.5 mL of ClF_5 and BrF_5, respectively, at room temperature. Excess ClF_5, BrF_5, and volatile side products (i.e., $[ClF_4][AsF_6]$ and $[BrF_4][AsF_6]$) were removed under dynamic vacuum at ambient temperature, and the product purities were checked by Raman spectroscopy. The products were stored under UHP Ar at −78 °C until used, and any transfers of these materials were made under the N_2 atmosphere of a drybox.

(c) $[ClF_6][Sb_2F_{11}]$ and $[BrF_6][Sb_2F_{11}]$. The salts $[ClF_6][Sb_2F_{11}]$ and $[BrF_6][Sb_2F_{11}]$ were prepared by transferring the AsF_6^- salts of ClF_6^+ and BrF_6^+ into solutions containing a slight excess of SbF_5 (i.e. $>2SbF_5$:AsF_6^-) in anhydrous HF in a T-shaped FEP reactor equipped with a stainless steel valve. The AsF_5 and excess SbF_5 were removed by decanting the cold supernatant into the side arm of the reactor, which was cooled to −196 °C and sealed off under vacuum. The product was dried under dynamic vacuum at −70 °C.

(d) $[IF_6][Sb_3F_{16}]$. The salt, $[IF_6][Sb_3F_{16}]$, was prepared by condensing IF_7 (1.871 g, 7.20 mmol) at −196 °C directly onto neat

(99) Drake, G. W.; Dixon, D. A.; Sheehy, J. A.; Boatz, J. A.; Christe, K. O. *J. Am. Chem. Soc.* **1998**, *120*, 8392.
(100) Christe, K. O.; Sanders, J. C. P.; Schrobilgen, G. J.; Wilson, W. W. *J. Chem. Soc., Chem. Commun.* **1991**, *13*, 837.
(101) Bertolini, J. C. *J. Emerg. Med.* **1992**, *10*, 163.
(102) Peters, D.; Mietchen, R. *J. Fluorine Chem.* **1996**, *79*, 161.
(103) Segal, E. B. *Chem. Health Saf.* **2000**, 19.
(104) Casteel, W. J., Jr.; Kolb, P.; LeBlond, N.; Mercier, H. P. A.; Schrobilgen, G. J. *Inorg. Chem.* **1996**, *35*, 929.
(105) Mercier, H. P. A.; Sanders, J. C. P.; Schrobilgen, G. J.; Tsai, S. S. *Inorg. Chem.* **1993**, *32*, 386.
(106) Pilipovich, D.; Maya, W.; Lawton, E. A.; Bauer, H. F.; Sheehan, D. F.; Ogimachi, N. N.; Wilson, R. D.; Gunderloy, F. C., Jr.; Bedwell, V. E. *Inorg. Chem.* **1967**, *6*, 1918.
(107) Ruff, O.; Keim, R. *Z. Anorg. Allg. Chem.* **1930**, *193*, 176.
(108) Gillespie, R. J.; Schrobilgen, G. J. *Inorg. Chem.* **1976**, *15*, 22.
(109) LeBlond, N.; Dixon, D. A.; Schrobilgen, G. J. *Inorg. Chem.* **2000**, *39*, 2473.
(110) Emara, A. A. A.; Schrobilgen, G. J. *Inorg. Chem.* **1992**, *31*, 1323.

SbF_5 (ca. 10 g) in a Kel-F reaction vessel followed by condensation of anhydrous HF (ca. 5 mL). The reaction mixture was warmed to −78 °C followed by slow warming over a period of 30 min to room temperature, whereupon the reaction mixture was agitated and allowed to stand for several hours prior to removal of the HF at −78 °C and excess SbF_5 at room temperature under dynamic vacuum. The yield of $[IF_6][Sb_3F_{16}]$ was 6.415 g (theoretical, 6.550 g).

X-ray Crystallography. (a) Crystal Growth. Crystals of $[ClF_6][Sb_2F_{11}]$, $[BrF_6][Sb_2F_{11}]$, and $[IF_6][Sb_2F_{11}]$ were grown by slowly lowering the temperature of anhydrous HF solutions of $[ClF_6][Sb_2F_{11}]$, $[BrF_6][Sb_2F_{11}]$, and $[IF_6][Sb_3F_{16}]$, respectively, from 0 to −70 °C, as previously described.[92]

(b) Crystal Mounting and Data Collection. Crystals of $[ClF_6][Sb_2F_{11}]$ (−130 °C), $[BrF_6][Sb_2F_{11}]$ (−130 °C), and $[IF_6][Sb_2F_{11}]$ (−173 °C) (McMaster University) were mounted on glass fibers using perfluorinated polyether oils as an adhesive at −110 ± 5 °C as previously described.[111] The crystals were then centered on a P4 Siemens diffractometer, equipped with a Siemens SMART 1K CCD area detector and a rotating molybdenum anode ($\lambda_{K\alpha}$ = 0.71073 Å, monochromated by a graphite crystal) and controlled by SMART.[112] The distance between the crystal and the detector face was 4.987 cm, and the collection of data was performed using 512 × 512 pixel modes using 2 × 2 pixel binning. The raw diffraction data was integrated in three dimensions using SAINT+,[113] which applied Lorentz and polarization corrections to the integrated spot intensities. Scaling of the integrated data was performed with SADABS,[114] which applied decay corrections and an empirical absorption correction on the basis of the intensity ratios of redundant reflections. The structure of $[IF_6][Sb_2F_{11}]$ was determined at −100 °C (University of Southern California) by use of a Kappa CCD (1152 H 1242 Pixel) diffractometer and Mo Kα radiation. The data for this structure were collected using the DENZO[115] and SCALEPACK[116] software packages.

(c) Solution and Refinement. The program XPREP[117] was used to confirm the unit cell dimensions and the space group. Direct methods were used to locate the heavy atoms (Sb, Cl, Br, I), and the fluorine positions were identified in successive difference Fourier syntheses. Final refinements were obtained using data that had been corrected for absorption by introducing an extinction coefficient and optimized using anisotropic thermal parameters.

NMR Spectroscopy. The ^{35}Cl (49.042 MHz), ^{37}Cl (40.823 MHz), ^{79}Br (125.561 MHz), ^{81}Br (135.348 MHz), and ^{127}I (100.400 MHz) spectra of $[ClF_6][AsF_6]$ (0.17 M), $[BrF_6][AsF_6]$ (0.077 M), and $[IF_6][Sb_3F_{16}]$ (0.065 M) in HF solvent were recorded on a Bruker DRX-500 (11.7438 T) spectrometer operating in unlocked mode (field drift < 0.1 Hz h^{-1}) using a 5 mm broad band probe at 27 °C. Pulse widths of 31.00, 29.25, 13.00, 13.00, and 16.75 μs were used for ^{35}Cl, ^{37}Cl, ^{81}Br, and ^{127}I, respectively. The spectra of the solutions were recorded in 4K ($^{35,37}Cl$), 8K ($^{79,81}Br$), and 32K (^{127}I) memories prior to zero filling the data to 8K, 16K, and 64K, respectively, and transforming the data. The spectral widths (Hz) of the ^{35}Cl (4883), ^{37}Cl (3255), ^{79}Br (20000), ^{81}Br (50000), and ^{127}I (69930) spectra yielded acquisition times of 0.419, 0.629, 0.205, 0.082, and 0.234 s, respectively. The spectral resolutions of the ^{35}Cl, ^{37}Cl, ^{81}Br, and ^{127}I spectra were 1.19, 0.80, 2.44, 6.10, and 2.13 Hz/data point, respectively. The spectra of the solutions were externally referenced at 27 °C to aqueous solutions of KCl, KBr, and KI extrapolated to infinite dilution. The T_1-relaxation times of the central halogens in the XF_6^+ cations were determined for the ^{19}F-coupled spectra by the spin-inversion-recovery method with delay time (τ) ranges of 0.100−3.00 s ($^{35,37}Cl$), 0.100−100 ms ($^{79,81}Br$), and 0.100−30 ms (^{127}I) and employed the spectral parameters used for the 1-D spectra. The T_1-relaxation times were determined by plotting the intensity of the central peak, I_c, of the septet versus τ, and fitting the data to the exponential relation, $I_c = a + be^{-\tau/T_1}$, where a, b, and T_1 were refined as independent variables.

Calculations. The energy-minimized gas-phase structures, vibrational frequencies, atomic charges, Mayer bond orders, and valencies of ClF_6^+, BrF_6^+, and IF_6^+ were calculated at the HF, MP2, and local density function (SVWN)[118] levels of theory using Gaussian 98.[119] The DZVP basis set was used in each case.[120]

The electron localization function (ELF) calculations were completed with TopMod,[121] using the Silvi−Savin approach to chemical bonding,[80] which is based on a topological analysis of the gradient field of the ELF. This analysis achieves a partition of the space into basins of the gradient field maxima or attractors. The method has also been briefly reviewed recently,[122] and a detailed description of the method and nomenclature can be found in ref 123. Small asymmetric artifacts appear in the integrated data which arise from the numerical grids employed in the TopMod code. Extra fine grids would remove these discrepancies, but the additional computational cost leading to extra precision are not expected to significantly alter the interpretations.[122]

Acknowledgment. This paper is dedicated to our friend and colleague Professor Ronald J. Gillespie on the occasion of his 80th birthday and in recognition of his many outstanding contributions across a broad spectrum of chemistry. We thank the donors of the Petroleum Research Fund,

(111) Gerken, M.; Dixon, D. A.; Schrobilgen, G. J. *Inorg. Chem.* **2000**, *39*, 4244.
(112) *SMART*, version 5.054; Siemens Energy and Automation Inc.: Madison, WI, 1999.
(113) *SAINT+*, version 6.01; Siemens Energy and Automation Inc.: Madison, WI, 1999.
(114) Sheldrick, G. M. SADABS (Siemens Area Detector Absorption Corrections), personal communication, 1998.
(115) Kappa CCD package by Nonius B.V., Roentgenweg 1, Delft, The Netherlands.
(116) Otwinowsky, Z.; Minor, W. *Methods Enzymol.* **1997**, *276*, 307.
(117) Sheldrick, G. M. *SHELXTL*, version 5.1; Siemens Analytical X-ray Instruments Inc.: Madison, WI, 1998.
(118) Vosko, S. H.; Wilk, L.; Nusair, M. *Can. J. Phys.* **1980**, *58*, 1200.
(119) Frisch, M. J.; Trucks, G. W.; Schlegel, H. B.; Scuseria, G. E.; Robb, M. A.; Cheeseman, J. R.; Zakrzewski, V. G.; Montgomery J. A., Jr.; Stratmann, R. E.; Burant, J. C.; Dapprich, S.; Millam, J. M.; Daniels, A. D.; Kudin, K. N.; Strain, M. C.; Farkas, O.; Tomasi, J.; Barone, V.; Cossi, M.; Cammi, R.; Mennucci, B.; Pomelli, C.; Adamo, C.; Clifford, S.; Ochterski, J.; Petersson, G. A.; Ayala, P. Y.; Cui, Q.; Morokuma K.; Malick D. K.; Rabuck A. D.; Raghavachari, K.; Foresman, J. B.; Ciosloski, J.; Ortiz, J. V.; Stefanov, B. B.; Lui, G.; Liashenko, A.; Piskorz, P.; Komaromi, I.; Gomperts, R.; Martin, R. L.; Fox, D. J.; Keith T.; Al-Laham, M. A.; Peng, C. Y.; Nanayakkara, A.; Gonzalez, C.; Challacombe, M.; Gill, P. M. W.; Johnson, B.; Chen, W.; Wong, M. W.; Andres, J. L.; Gonzalez, C.; Head-Gordon, M.; Replogle, E. S.; Pople, J. A. *Gaussian 98*, revision A.4; Gaussian, Inc.: Pittsburgh, PA, 1998.
(120) Basis sets were obtained from the Extensible Computational Chemistry Environment Basis Set Database, version 6/19/03, as developed and distributed by the Molecular Science Computing Facility, Environmental and Molecular Sciences Laboratory, which is part of the Pacific Northwest Laboratory, P.O. Box 999, Richland, WA 99352, and funded by the U.S. Department of Energy. The Pacific Northwest Laboratory is a multiprogram laboratory operated by Battelle Memorial Institute for the U.S. Department of Energy under Contract DE-AC06-76RLO 1830.
(121) Noury, S.; Krokidis, X.; Fuster, F.; Silvi, B. *TopMod*; Laboratoire de Chimie Théorique, University of Paris VI: Paris, 1998.
(122) Malcolm, N. O. J.; Gillespie, R. J., Popelier, P. L. A. *J. Chem. Soc., Dalton Trans.* **2002**, 3333.
(123) Savin, A.; Silvi, B.; Colonna, F. *Can. J. Chem.* **1996**, *74*, 1088.

administered by the American Chemical Society, for support of this work under ACS-PRF No. 37128-AC3 (G.J.S.) and the Natural Sciences and Engineering Research Council of Canada for a postgraduate scholarship and McMaster University for a Dalley Fellowship (J.F.L.). The National Science Foundation and Air Force Office of Scientific Research financially supported the work at the University of Southern California (K.O.C.).

Supporting Information Available: The nonaveraged values of N_i, λ, and $\sigma^2(N_i)$ for the ClF_6^+, BrF_6^+, and IF_6^+ cations (Table S1) and the X-ray crystallographic files in CIF format for the structure determinations of [ClF_6][Sb_2F_{11}], [BrF_6][Sb_2F_{11}], and [IF_6][Sb_2F_{11}]. This material is available free of charge via the Internet at http://pubs.acs.org.

IC040015O